Functional Imaging of Neural Responses to Expectancy and Experience of Monetary Gains and Losses

Hans C. Breiter,[1,2,3,6] Itzhak Aharon,[1,2]
Daniel Kahneman,[5] Anders Dale,[2]
and Peter Shizgal[4]
[1] Motivation and Emotion Neuroscience Center
Department of Radiology
[2] MGH-NMR Center
Department of Radiology
[3] Department of Psychiatry
Massachusetts General Hospital and
Harvard Medical School
Charlestown, Massachusetts 02129
[4] Center for Studies in Behavioral Neurobiology
Concordia University
Montreal, Quebec H3G 1M8
Canada
[5] Woodrow Wilson School of Public
   and International Affairs
Princeton University
Princeton, New Jersey 08544

Summary

Neural responses accompanying anticipation and experience of monetary gains and losses were monitored by functional magnetic resonance imaging. Trials comprised an initial "prospect" (expectancy) phase, when a set of three monetary amounts was displayed, and a subsequent "outcome" phase, when one of these amounts was awarded. Hemodynamic responses in the sublenticular extended amygdala (SLEA) and orbital gyrus tracked the expected values of the prospects, and responses to the highest value set of outcomes increased monotonically with monetary value in the nucleus accumbens, SLEA, and hypothalamus. Responses to prospects and outcomes were generally, but not always, seen in the same regions. The overlap of the observed activations with those seen previously in response to tactile stimuli, gustatory stimuli, and euphoria-inducing drugs is consistent with a contribution of common circuitry to the processing of diverse rewards.

Introduction

The hubbub on a stock exchange trading floor and the contagious excitement elicited by large lottery jackpots are but two examples of the powerful emotions that accompany the anticipation and experience of monetary gains and losses. There has been a resurgence of interest in emotion among neuroscientists (Damasio, 1994; LeDoux, 1996; Rolls, 1999), and neuroimaging methods have been applied to map brain responses to emotionally and motivationally salient stimuli in humans (Breiter et al., 1996a, 1997; Morris et al., 1996; Stein et al., 1998). In several of these studies, brain hemodynamic changes were monitored during performance of game-playing

[6] Correspondence: hbreiter@partners.org

tasks with monetary payoffs (Breiter et al., 1996b; Elliott et al., 2000; Knutson et al., 2000; O'Doherty et al., 2001; Thut et al., 1997).

Emotions have figured prominently in recent empirical and theoretical work on evaluation and choice. For example, Mellers and coworkers have shown that the emotional response to the outcome of a gamble depends on the perceived value and likelihood of both the obtained outcome and its alternatives (Mellers et al., 1997). Thus, it feels better to receive $0 from a gamble when the unobtained alternative is a gain of $10 than when the alternative is a gain of $90; winning $50 feels better when the odds of doing so are 10% than when the odds are 90%. The influence of what might have been on the response to an outcome is said to be "counterfactual." Mellers et al. (1999) have shown that counterfactual influences also affect anticipated feelings. Their subjects expect to feel worse upon winning $0 when the alternative is $90 than when the alternative is only $10.

The orderly emotional responses to gambles described by Mellers et al. (1999, 1997) provide a rich framework for functional neuroimaging studies. By varying the obtained and unobtained outcomes, the strength and sign of emotional responses can be manipulated using visual stimuli easily presented in the functional neuroimaging setting. Comparing the neural correlates of the evoked emotions to those associated with natural goal objects and to drugs of abuse could shed light on the generality of the anticipatory and evaluative mechanisms.

There are interesting parallels between the counterfactual comparisons and anticipatory emotional responses documented in humans by Mellers et al. and results of electrophysiological studies of midbrain dopaminergic neurons in monkeys carried out by Schultz and coworkers (Schultz et al., 1992, 1993, 1997; Schultz and Romo, 1990). After the monkey has learned that a stimulus predicts the imminent availability of reward, presentation of this stimulus triggers a burst of firing in the dopaminergic neurons. This anticipatory burst is not tied to the preparation of an operant response but rather to the expectation of a positive outcome. During delivery and consumption of the reward, the activity of the dopamine neurons appears to reflect a comparison between expectation and outcome. When the expected reward is obtained, the dopaminergic neurons maintain their baseline activity, but when the reward is omitted, firing decreases. The inhibition due to reward omission can be construed as the result of a counterfactual contrast between the positive outcome that was expected and the null outcome that was obtained instead. Similarly, the activation of dopaminergic neurons by unexpected but not by expected rewards may bear some relation to the more positive emotional responses of humans to low-probability gains than to high-probability gains of the same magnitude.

Among the many projection fields of the ventral tegmental (VT) dopamine neurons are the orbitofrontal cortex (GOb), nucleus accumbens (NAc), amygdala, sublenticular extended amygdala (SLEA) of the basal forebrain,

and hypothalamus (Heimer et al., 1997; Lindvall and Bjorklund, 1974; Lynd-Balta and Haber, 1994). All of these regions project back to the area from which the ascending dopaminergic projections arise. Thus, signals related to reward expectancy and to differences between expectancies and outcomes may be distributed in parallel by dopaminergic neurons to many cortical and subcortical cell groups; in turn, projections converging on midbrain dopamine neurons from many different regions could shape the responses of these cells to predictive stimuli and delivered outcomes. Indeed, an extensive electrophysiological literature relates cell firing in dopaminergic terminal fields, such as the GOb, NAc, amygdala, SLEA, and hypothalamus, to the expectation and experience of positive outcomes and, in some cases, to negative ones as well (Bordi and LeDoux, 1992; Hollerman et al., 1998; Mora et al., 1977; Ono et al., 1986; Ono et al., 1981; Rolls et al., 1976; Schoenbaum et al., 1998, 2000; Schultz et al., 1992; Tremblay and Schultz, 1999). Recent functional neuroimaging studies in humans have complemented and extended the animal research by describing patterns of brain activation that accompany delivery of cocaine to habitual users of this drug (Breiter et al., 1997, 1998; Breiter and Rosen, 1999), nicotine to chronic smokers (Stein et al., 1998), and aversive or pleasant tastants (Small et al., 2001; Zald et al., 1998) or pleasant tactile stimuli (Francis et al., 1999) to normal subjects. However, these studies leave open the question of whether the GOb, NAc, amygdala, SLEA, hypothalamus, and VT respond in a coordinated fashion during the expectation and experience of positive and negative outcomes.

The purpose of the present neuroimaging study was to map human hemodynamic responses to the expectation and experience of monetary gains and losses in a testing paradigm based on well-established psychological principles underlying anticipation and evaluation under uncertainty (Kahneman and Tversky, 1979; Mellers et al., 1997, 1999). The analysis was focused on the six brain regions discussed above: the GOb, NAc, amygdala, SLEA, hypothalamus, and VT. We wished to determine whether monetary prospects and outcomes activate these regions in a manner reminiscent of the responses seen in prior studies employing tastants, tactile stimuli, and euphoria-inducing drugs. If so, do the magnitudes of the hemodynamic responses track the expected and obtained monetary values? It was also of interest to ascertain whether both anticipatory and evaluative responses are seen in the same regions, as has often been the case in prior animal experiments, or whether responses to monetary prospects and outcomes in humans are segregated anatomically at the scale provided by the measurement system. To ensure high spatial resolution, neuroimaging was performed using high-field (3 T) functional magnetic resonance imaging (fMRI). Use of fMRI also provided the temporal resolution required to distinguish anticipatory responses to prospects from outcome responses to gains and losses.

Two psychological principles underlying the design of this study are derived from prospect theory (Kahneman and Tversky, 1979). According to one of these principles, the evaluation of a risky prospect, such as a gamble, depends little on cumulative winnings or losses (the "asset position") but is framed instead as a gain or loss with respect to a neutral point. This principle lends legitimacy to the practice of averaging all responses to a given gamble in a long counterbalanced sequence of different gambles, and it suggests that stimuli should be configured so as to emphasize gains and losses rather than asset position. According to the second principle, the impact of a loss exceeds the impact of a gain of equal magnitude. If so, larger gains than losses should be used so as to compensate for the asymmetry in emotional responses. A third principle, derived from decision affect theory, concerns the importance of counterfactual comparisons in emotional responses to prospective and obtained outcomes (Mellers et al., 1997, 1999).

The subjects were informed that they would be participating in a game of chance during the fMRI session. A $50 endowment was provided, and the subjects were told that during the game, they might lose some or all of this stake, retain it, or increase it. Experimental trials were divided into two phases (Figure 1a). During the initial "prospect" (expectancy) phase, one of three spinners (Figure 1b) was presented. The spinners were subdivided into three equal sectors—each labeled with a different monetary value. The image of an arrow rotated around the center of the spinner during the prospect phase, and the arrow stopped at one sector at the start of the "outcome" phase. The subjects understood that the amount of money indicated on that sector would be added to or subtracted from their total, but the cumulative winnings or losses were not displayed. The timing of the prospect and outcome phases made it possible to distinguish hemodynamic signals associated with anticipation from those associated with the experience of outcomes. During control trials, the display consisted of a stationary fixation point. The design followed a single-trial format, and the trial sequence was counterbalanced.

Expectations and counterfactual comparisons were established by the composition of the three spinners (*good*: $10, $2.50, $0; *intermediate*: $2.50, $0, −$1.50; *bad*: $0, −$1.50, −$6). The use of multiple gains and losses made it possible to determine whether hemodynamic responses tracked the magnitude and sign of the outcomes; inclusion of the null outcome ($0) on all three spinners made it possible to assess how counterfactual comparisons affected the hemodynamic response.

Results

Functional Imaging Data

The analysis proceeded in three phases. First, functional regions of interest (ROIs) were identified in a correlation analysis between an impulse function and data selectively averaged on a trial-by-trial basis (Dale and Buckner, 1997; Dale, 1999). The basis for this selection was the presence of overall hemodynamic changes linked to the prospect and/or outcome phases, averaged over both trial types and subjects (a). Second, the time course of signal change in each of the clusters identified as ROIs was analyzed in individual subjects for each spinner and outcome (b). Two types of analyses were performed on ROI data, including evaluation of whether or not the 95% confidence bands crossed the zero baseline, and

computation of an analysis of variance with post-hoc planned contrasts. Third, the analysis was extended beyond the ROIs by searching for clustered voxels, in other brain regions, whose hemodynamic responses were tied to differences between extreme and intermediate conditions (c) (e.g., the best outcome on a given spinner and the middle outcome).

Foci of Signal Change in Targeted Anatomic Regions

Twelve subjects had motion-correctable data. For selectively averaged data from these subjects, ten ROIs were identified from correlation of the averaged prospect time course with a γ function. Four of these ROIs were located in subcortical regions: the right nucleus accumbens (NAc), left amygdala, right hypothalamus, and right ventral tegmentum (VT). An additional six ROIs, in which generalized prospect responses were seen, were located in the orbital gyrus (GOb), two in the left hemisphere, and four in the right (Table 1; Figure 2).

Six additional ROIs were identified from correlation of the averaged outcome time course with the γ function. Two of these ROIs were located in subcortical regions: the right sublenticular extended amygdala of the basal forebrain (SLEA) and the right amygdala. An additional four ROIs, in which generalized outcome responses were seen, were located in the GOb, three in the left hemisphere, and one in the right (see Table 1; Figure 2).

Robust Analysis of Signal Time Courses

Robust analysis of signal from the 16 ROIs was carried out using individual time courses for each trial type, and with statistical methods resistant to the contaminating effects of outliers.

Prospect/Expectancy Time Courses

Description and Comparison to Baseline. The five ROIs with the highest signal-to-noise ratios (Table 2) during the prospect phase (2–6 s time points) were the NAc, SLEA, hypothalamus, VT, and GOb(5), all in the right hemisphere (Figure 3). In these ROIs, there were relatively strong prospect responses to the good spinner, and the 95% confidence intervals around the mean time course clears the zero baseline at multiple time points (Table 1). In several of these clusters, weaker responses were seen to the intermediate and bad spinners, and in the SLEA and GOb(5), the peaks of the prospect responses are ordered according to the expected value of the spinner. Predominant responses to the good spinner were seen in four additional GOb ROIs in the right hemisphere (Table 1).

The signals from the left amygdala (ROI #11) show a contrasting pattern to the other responses in Figure 3. In this case, there is a biphasic response, which deviates reliably from the baseline for the bad spinner, and a minimal response to the other spinners. Predominant responses to the bad spinner were seen in three left-hemisphere GOb ROIs (Table 1).

The distinction between the prospect and outcome responses can be seen with particular clarity in the time courses in Figure 4a (and Figure S1 [see supplemental data at http://www.neuron.org/cgi/content/full/30/2/619/DC1]). Note that the responses are similar during the prospect phase, when the displays for the three trial types were identical, and the responses diverge during the outcome phase, when the displays differed.

The expectancy phase time courses deviated reliably from the baseline at a total of 38 time points; at 37 of these, the deviations were in the positive direction. Four clusters in subcortical or brainstem regions of the right hemisphere, the NAc, SLEA, hypothalamus, and VT, account for 24 of the reliable deviations from baseline.

The time to peak measures varied across prospect responses (Table 2). Signals from subcortical and brainstem structures with robust simultaneous 95% confidence bands that cleared the baseline, peaked at 4 s in 10 of 13 cases. In contrast, several of the signals that peaked later were recorded in GOb ROIs (see Figure S2 [see supplemental data at http://www.neuron.org/cgi/content/full/30/2/619/DC1]).

ANOVAs and Contrasts. Spinner and time point served as the predictors in the two-way ANOVA of the prospect responses. As shown in Table 1, the effect of spinner on the prospect responses met the significance criterion in three subcortical regions of the right hemisphere, the NAc (robust $F_{[2, 315]} = 6.46$, $p = 0.0018$), SLEA (robust $F_{[2, 315]} = 9.27$, $p = 0.0001$), and hypothalamus (robust $F_{[2, 315]} = 9.1$, $p = 0.0001$). In addition, a significant effect was seen in one cortical ROI, GOb(10) $-$ (robust $F_{[2, 315]} = 16.13$, $p < 0.00005$). The spinner by time point interaction met the significance criterion in three ROIs: hypothalamus (robust $F_{[4, 315]} = 5.95$, $p = 0.0001$), amygdala(11) ($F_{[4, 315]} = 5.52$, $p = 0.0003$), and GOb(1) (robust $F_{[4, 315]} = 4.11$, $p = 0.0029$).

Post-hoc contrasts, carried out to determine the source of the main effects and interactions in the ANOVAs, are summarized in Table 3. These contrasts demonstrate that many of the orderly differences between the time courses seen in Figure 3a (i.e., ordering of response magnitude according to the expected value of the spinners) cross the threshold for statistical reliability. In the case of the NAc, SLEA, and hypothalamus, the magnitude of responses to some spinners with higher expected values (good and/or intermediate) exceeded the magnitude of responses to the spinner with the lowest expected value (bad). An opposite pattern was seen in the responses recorded from ROIs in the amygdala(11), GOb(1), and GOb(10). In these cases, the response to the bad spinner was reliably stronger than the response to the good and/or intermediate spinners at certain time points (Table 3).

Outcome Time Courses

Description and Comparison to Baseline. As in the case of the prospect responses, the outcome phase responses (8–12 s time points) were compared to the zero baseline by means of robust simultaneous 95% confidence intervals (Table 1). Reliable deviations from the zero baseline are observed for the NAc (11 time points), SLEA (14 time points), hypothalamus (six time points), and GOb(4) (three time points) confirming the visual impression conveyed by Figures 4a and 4b.

Four of the time courses shown in Figures 4a and 4b deviate reliably from the baseline at all three time points, and eight do so at two neighboring time points. Of the remaining 16 cases in which the robust simultaneous 95% confidence interval cleared the baseline, there was only one instance in which the deviation was seen at more than a single time point.

The good-spinner outcome phase responses recorded from the VT are ordered according to the monetary value of the outcomes, as is the case in the NAc,
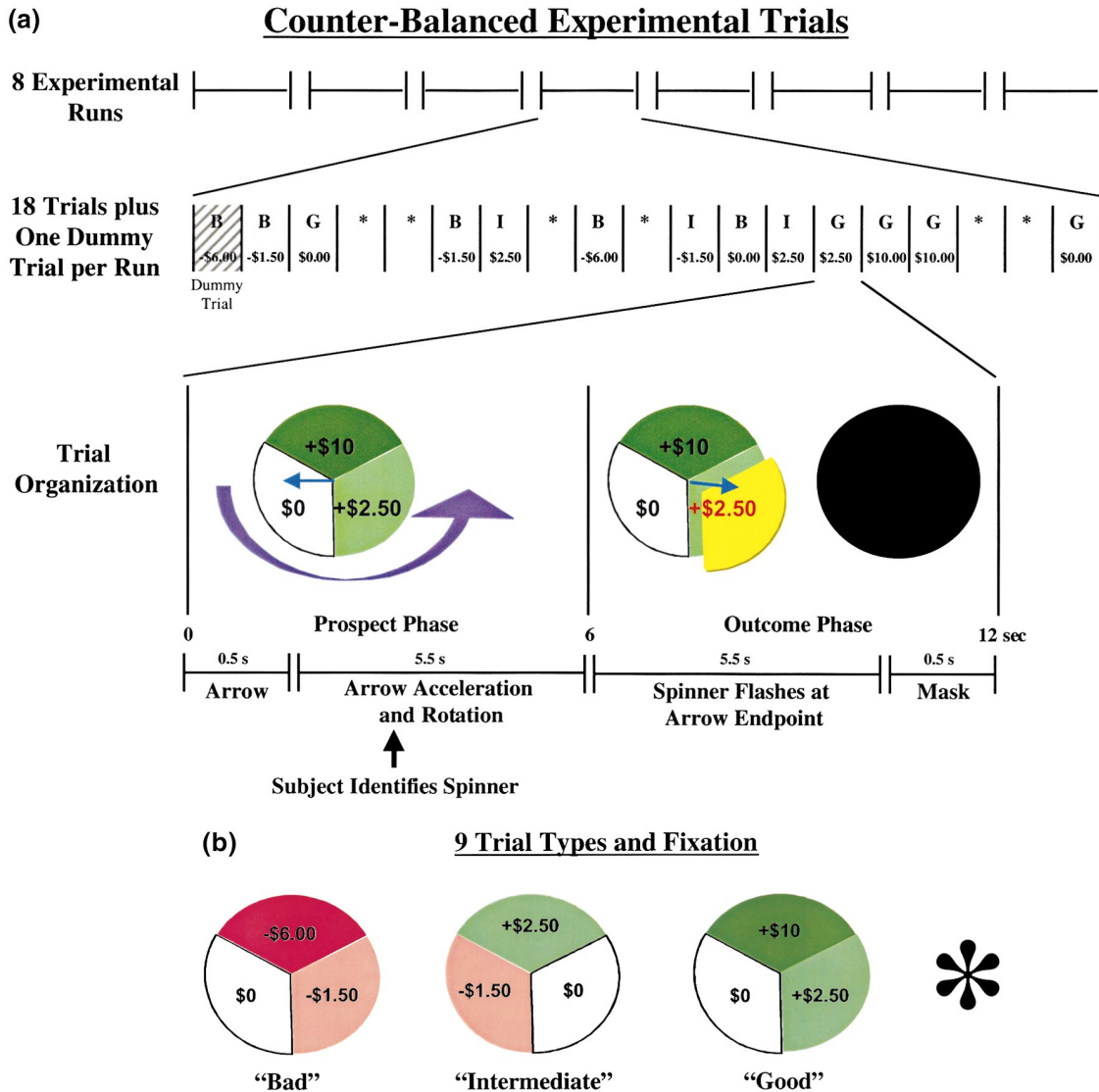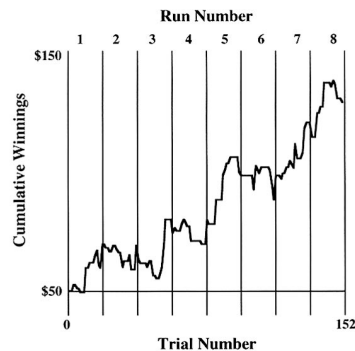
Figure 1. Experimental Design

As diagrammed in Figure 1a, the experiment consisted of eight runs, with 19 trials per run. The first trial in each run was a "dummy" trial, included to ensure complete first-order counterbalancing with regard to hemodynamic carryover effects for each trial type over the entire experiment. The nine trial types representing the spinner * outcome combinations were presented 12 times each, and the fixation point baseline was presented 36 times. (These counts exclude the dummy trials.) Trials were subdivided into a "prospect phase" and an "outcome phase," each of 6 s duration. During the "prospect phase," subjects initially saw a colored "spinner" on which a superimposed arrow appeared after 0.5 s and began to rotate. It accelerated and then continued spinning for 5.5 s. During this time, subjects were instructed to push a designated button to identify the spinner. At 6 s, the arrow stopped on one of the three sectors, and that sector flickered for 5.5 s to indicate

Table 1. Functional Foci in A Priori Regions of Interest

Anatomy	Coordinates			Confidence Intervals Clearing Baseline		Time Points Clearing Baselines				ANOVA	
	R/L	A/P	S/I	Prospects	Outcomes	Prospects		Outcomes		Prospects	Outcomes
						(+)	(−)	(+)	(−)		
Frontal Lobe											
GOb(1)[+] (L)	−25	47	−18	B	2, 8	1	0	1	1	SP*TP	TT
GOb(2)[+] (R)	15	34	−21	G, I	1	2	0	1	0	—	—
GOb(3)[+] (L)	−12	66	−6	—	—	0	0	0	0	—	—
GOb(4)[+] (R)	18	19	−25	—	1, 9	0	0	3	0	—	TT
GOb(5)[+] (R)	6	59	−12	G	3	2	0	1	0	—	TT
GOb(6)[+] (R)	25	59	−18	G	2, 8	2	0	2	0	—	TT*TP
GOb(7)[++] (L)	−34	38	−18	B	2	1	0	1	0	—	—
GOb(8)[++] (L)	−12	31	−21	G	6	1	0	1	0	—	TT
GOb(9)[++] (R)	28	44	−12	G, B	—	2	0	0	0	—	—
GOb(10)[++] (L)	−25	13	−9	B	2, 3, 7	1	0	1	2	SP	TT, TT*TP
Temporal Lobe											
Amygdala(11)[+] (L)	−18	3	−15	B	5	1	1	0	1	SP*TP	TT
Amygdala(12)[++] (R)	21	−3	−21	—	9	0	0	0	2	—	TT
Subcortical Gray											
NAc(13)[+] (R)	12	16	−6	G, I, B	1–3, 6, 7, 9	7	0	0	11	SP	TT, TT*TP
SLEA(14)[++] (R)	18	0	−6	G, I, B	1–3, 6–9	7	0	0	14	SP	TT
Hypothalamus(15)[+] (R)	9	−3	−6	G, I, B	3, 6, 9	4	0	1	5	SP, SP*TP	TT
Brainstem											
VT(16)[+] (R)	12	−18	−12	G, I, B	3	6	0	0	1	—	TT

Table 1 summarizes the anatomic location of regions of interest (ROIs), deviations of BOLD signals from baseline, and ANOVA results. The listed anatomic structures are followed by a ROI number in brackets; these numbers are carried through Tables 2–4 and Figures 2–5 and S1–S5. The listed anatomic structure is also followed by a superscripted symbol (either a[+] or a[++]), indicating which epoch of data (either prospect/expectancy [+] or outcome data [++] epochs) produced the ROI in this region. The hemispheric laterality is further denoted by a (L) or (R). "Coordinates" denotes the Talairach coordinates using the atlas of Talairach and Tournoux (1988) of the voxel with the strongest p value at the center of each of the 16 ROIs. Coordinates are expressed in mm from the anterior commissure: R/L, right (+)/left (−); A/P, anterior (+)/posterior (−); S/I, superior (+)/inferior (−). "Change from Baseline" identifies ROIs in which the 95% confidence interval around the BOLD signal cleared zero. For the "Prospect" column, the spinner responsible for the deviation from zero is indicated by a "G," "I," or "B," for the good, intermediate, and bad spinners, respectively. For the "Outcomes" column, numerals refer to the trial type as follows: 1, 2, and 3 represent the $10, $2.50, and $0 outcomes, respectively, on the good spinner. For the intermediate spinner, 4, 5, and 6 represent the $2.50, $0, and −$1.50 outcomes, respectively, and 7, 8, and 9 represent the $0, −$1.50, and −$6 outcomes, respectively, on the bad spinner. "Time Points Clearing Baselines" lists how many time points reliably cleared the baseline for prospect and for outcome data. In both the "Prospects" and the "Outcomes" columns, + refers to positive deviations from zero, and − refers to negative deviations from zero. The "ANOVA" column lists the ROIs for which significant main effects or interactions were found. ROIs with nonsignificant results are designated by a dash (—). For the expectancy phase, ROIs with a significant main effect of spinner are indicated by "SP," and ROIs with a significant interaction of spinner and time point are indicated by "SP*TP." ROIs with significant main effects of trial type during the outcome phase are designated by "TT," whereas ROIs with significant interaction of trial type and time point are indicated by "TT*TP."

SLEA, and hypothalamus. In these cases, the ordering of the normalized BOLD signal during the outcome phase tracks the subjects' winnings. A strikingly different response pattern is seen for GOb(4) in Figure 4b, in which the BOLD signal grows during the outcome phase in response to the two most extreme outcomes: a $10 win following presentation of the good spinner and a $6 loss following presentation of the bad spinner. Deviations of outcome time courses from baseline, usually at single time points, were also seen in seven GOb foci and in the left amygdala (Table 1).

Overall, the outcome phase time courses differed reliably from the baseline at a total of 49 time points. Of these, 35 were in signals recorded from the six subcortical or brainstem clusters. Signals recorded from the right hemisphere account for 33 of these 35 time points,

and in 34 cases, the signals were below the baseline at the time points in question.

Figure 5 shows that in the NAc and SLEA ROIs, the BOLD response to the $0 outcome varied as a function of spinner. The most negative values are seen in the good-spinner response (triangles), in which case $0 was the worst of the three outcomes. More positive values were achieved by the bad-spinner response (inverse triangles), in which case $0 was the best of the three outcomes. The intermediate-spinner response (small circles) fluctuated near the zero baseline; in that case, $0 was the middle outcome.

ANOVAs and Contrasts. Spinner, outcome, and time point served as the predictor variables in the three-way ANOVA performed to determine whether the magnitude of the outcome responses varied as a function of out-

the amount won or lost. The spinner was then replaced by a black disc for 0.5 s as a mask before the next trial. Figure 1b shows the "good," "intermediate," and "bad" spinners. Monetary outcomes depicted on these spinners included $10, $2.50, $0, −$1.50, and −$6 as shown. The $2.50, $0, and −$1.50 outcomes were shared between all, or a subset, of the spinners. The sequence of trials was fixed, with the accumulation of monetary winnings beyond the initial endowment of $50 shown in the graph.
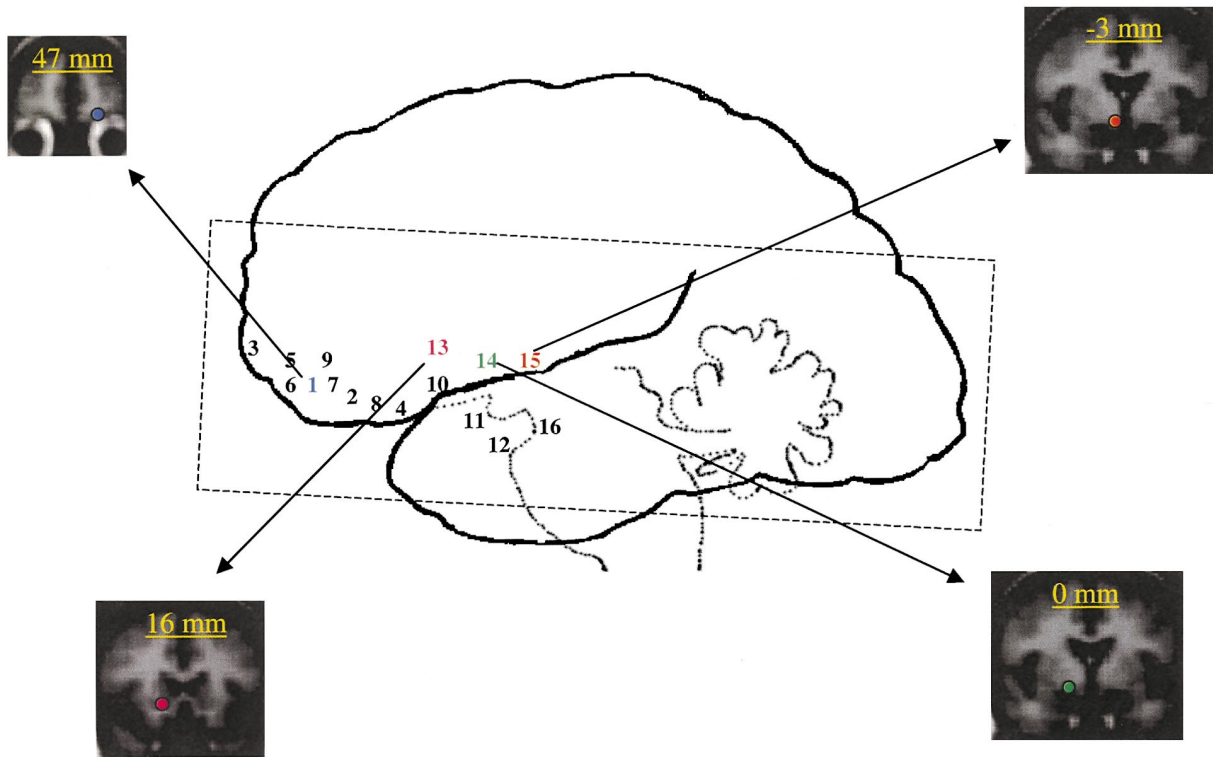
Figure 2. Foci of Signal Change

Scanning was performed using axial oblique 3 mm slices with 3.125 mm × 3.125 mm voxels. Brain coverage for the 18 slices approximated the dashed box. Target a priori regions included the nucleus accumbens (NAc), the sublenticular extended amygdala of the basal forebrain (SLEA), the amygdala, the hypothalamus, the ventral tegmentum of the midbrain (VT), and the orbital cortex (GOb). Sixteen foci of putative signal change were identified initially in averaged data. Four sample brain slices in gray tone are shown for the GOb, NAc, SLEA, and hypothalamus, with the ROI used for sampling fMRI signal from individuals depicted in color overlying the corresponding anatomic region.

come. Outcome was nested in spinner. As shown in Table 1, the effect of outcome on the outcome phase responses met the significance criterion in all six subcortical regions, as well as in five GOb ROIs. The F values range from 3.70 (VT) to 19.11 (NAc), and the corresponding p values from <0.00005 (NAc, hypothalamus, amygdala[11], and GOb[1]) to 0.0015 (VT); in all cases, there were 6° of freedom for outcomes and 297° of freedom for the within-cell error. The outcome by time point interaction met the significance criterion in the NAc (robust F[12, 297] = 5.58, p < 0.00005) as well as in GOb ROI #6 (robust F[12, 297] = 3.20, p < 0.0002) and ROI #10 (robust F[12, 297] = 4.61, p < 0.00005).

Table 4 summarizes the post-hoc contrasts carried out to determine the source of the main effects and interactions in the ANOVAs. As shown in Figure 4a, the outcome phase signals recorded in the NAc, SLEA, and hypothalamus in response to the $10 outcome on the good spinner are generally less negative than the responses to the $2.50 outcome, which are generally less negative than the response to the $0 outcome. The post-hoc contrasts demonstrate that several of these orderly differences between the time courses cross the threshold for statistical reliability, particularly in the cases of the good and intermediate spinners. The NAc, SLEA, and hypothalamus clusters, all located in subcortical regions of the right hemisphere, account for 15 of the

24 cases in which contrasts between outcome phase responses crossed the threshold for statistical reliability.

In two of the outcome phase responses for which the post-hoc contrasts crossed the threshold for statistical reliability, there is an opposite pattern to that in the NAc, SLEA, and hypothalamus, where responses to higher-valued outcomes tend to exceed responses to lower-valued outcomes. In cluster GOb(5), the responses to the most negative outcomes on the good and intermediate spinners reliably exceed the response to the middle outcome at one time point. A similar pattern is seen in amygdala(11), where the good-spinner response to the $0 outcome exceeds the response to the $2.50 outcome at the 8 s time point.

Post-Hoc Voxel-by-Voxel Correlational Analysis
Post-hoc voxel-by-voxel analysis was pursued on group averaged data to evaluate if brain regions not hypothesized to be active in the task were potentially active with the prospect/expectancy or outcome phases of the paradigm. The rationale for this post-hoc analysis was to facilitate the generation of future a priori hypotheses, and, thus, the results from it should be considered as secondary to the ROI results. All activations above a priori thresholds are listed (p < 4.73 × 10^{-5}), and activations meeting the Bonferroni threshold (p < 7.1 × 10^{-6}) are marked with an asterisk (*) in Tables S1–S8 (see supplemental data at http://www.neuron.org/cgi/content/

Table 2. Signal Quantitation For Prospect Data

Anatomy	Time to Peak (s)			Signal/Noise at Peak		
	Good	Inter	Bad	Good	Inter	Bad
Frontal Lobe						
GOb(1) (L)	—	—	4	—	—	3.6
GOb(2) (R)	6	6	—	4.1	3.1	—
GOb(3) (L)	—	—	—	—	—	—
GOb(4) (R)	—	—	—	—	—	—
GOb(5) (R)	4	—	—	6.5	—	—
GOb(6) (R)	6	—	—	3.7	—	—
GOb(7) (L)	—	—	2	—	—	4.0
GOb(8) (L)	4	—	—	3.1	—	—
GOb(9) (R)	4	—	2	3.2	—	2.2
GOb(10) (L)	—	—	2	—	—	3.1
Temporal Lobe						
Medial						
Amygdala(11) (L)	—	—	6	—	—	3.5
Amygdala(12) (R)	—	—	—	—	—	—
Subcortical Gray						
NAc(13) (R)	4	4	4	8.2	10.7	5.1
SLEA(14) (R)	4	4	4	7.0	4.8	2.9
Hypothalamus(15) (R)	6	4	2	5.7	4.5	2.8
Brainstem						
VT(16) (R)	2	4	4	4.9	3.6	3.2

Table 2 displays quantitative characteristics of expectancy phase signals. These data describe time courses whose upper and lower 95% confidence intervals clear zero. As in the previous table, the anatomic location of each ROI is listed under "Anatomy," with ROI# identifying the ROI for reference purposes. Under "Time to Peak (s)," the time to maximal signal change is listed for the response to each spinner in seconds. Under "Signal/Noise at Peak," a calculation comparable to a Z score is listed. This calculation is the ratio of the robust mean for the time point with maximal signal and the standard error of that mean. Given that we did not have "dummy" trials at the end of each run for potential carryover effects from the outcome of the last trial, we could only consider outcome effects for three time points and, thus, could not determine peaks in outcome time courses.

full/30/2/619/DC1). The post-hoc correlation analysis has a different emphasis than the ROI-based analysis in two fundamental ways. First, clusters of activation identified in the ROI-based analysis have multiple voxels contributing signal and adding power. Secondly, a pairwise contrast may be washed out when data from all nine trial types are averaged, as in the cluster-selection for the ROI-based analysis.

Prospect/Expectancies
Foci of positive signal change were noted for the good versus intermediate spinner comparison in lateral prefrontal and temporal cortex (Table S1 [see supplemental data]), whereas foci of negative signal change were noted for this comparison in inferior prefrontal cortex (i.e., GOb), and temporal cortex (Table S3 [see supplemental data]). In contrast, foci of negative signal change were observed for the bad versus intermediate spinner comparison in lateral prefrontal cortex and temporal cortex (Table S4 [see supplemental data]), whereas foci of positive signal change were noted in inferior prefrontal cortex and temporal cortex (Table S2 [see supplemental data]). For comparisons of good versus intermediate and bad versus intermediate spinners, activation in primary and secondary visual cortices was observed (see Tables S1–S4 [see supplemental data]). Subcortical gray structures were only activated for the comparison of the good versus intermediate spinners and included a left ventral striatum/nucleus accumbens activation (see Figure 6; note laterality difference from ROI # 13, Table 1) and a negative putamen activation.

Outcomes
In general, each spinner was associated with different patterns of signal change for gains versus losses. Thus, the $10 versus $2.50 comparison on the good spinner was associated with positive activation in the middle occipital gyrus, along with negative activation in the GOb, parahippocampus, hypothalamus, and lateral prefrontal cortex (Tables S5 and S7 [see supplemental data]). The $2.50 versus $0 comparison for the intermediate spinner was associated with foci of positive and negative signal change in primary plus secondary visual cortices (Tables S5 and S7 [see supplemental data]). Foci of positive signal change were associated with gains on the bad spinner ($0 versus −$1.50 comparison) in the GOb and visual cortex (Table S5 [see supplemental data]). Foci of negative signal change were also observed with the bad spinner in the anterior frontal cortex and GOb (Table S7 [see supplemental data]).

With regard to losses, the good spinner ($0 versus $2.50) was associated with positive signal change in thalamus and secondary visual cortex (Table S6 [see supplemental data]), but negative change in parahippocampus, thalamus, and secondary visual cortex (Table S8 [see supplemental data]). The intermediate spinner (−$1.50 versus $0) was associated with no positive signal changes (Table S6 [see supplemental data]) and negative primary visual cortex signal change (Table S8 [see supplemental data]). The bad spinner (−$6 versus −$1.50) was associated with foci of positive and negative secondary visual cortex activation, and negative
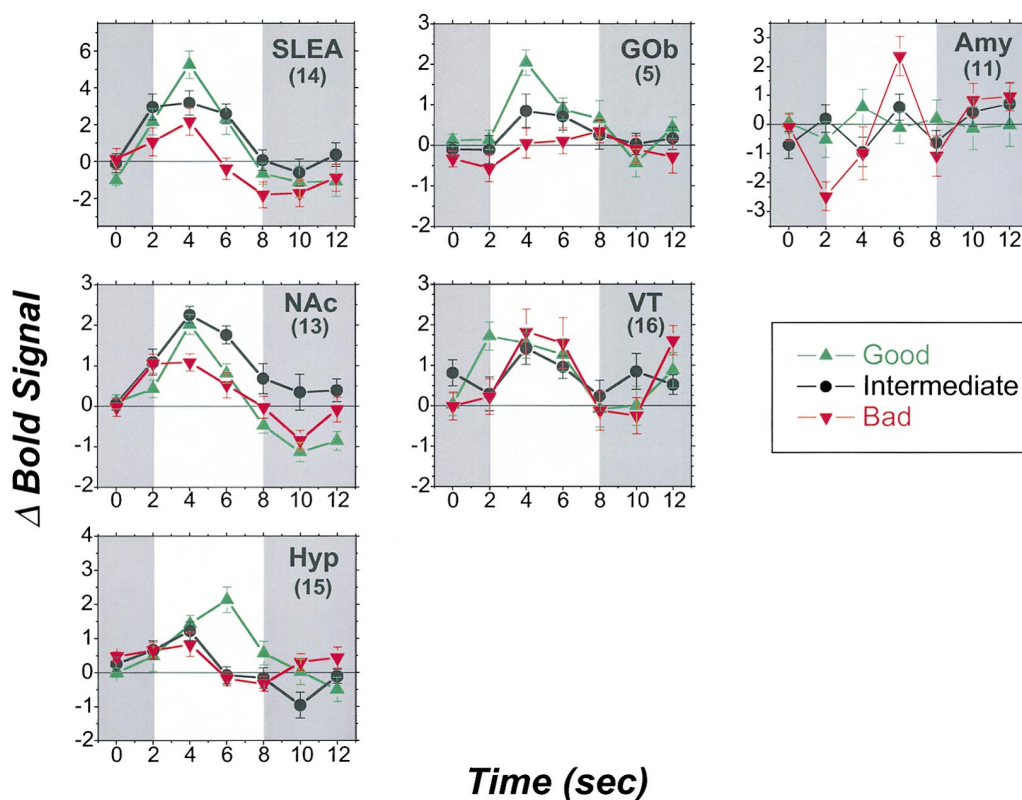
Figure 3. Prospect Phase Time Courses

Averaged fMRI signals are displayed for six ROIs. Signals were zeroed relative to the 8 s prestimulus epoch (see Figure S5 [supplemental data at http://www.neuron.org/cgi/content/full/30/2/619/DC1]). The time courses for the good (green), intermediate (black), and bad (red) spinners are displayed, with the white background marking the time window used in the analysis of the prospect responses and the remaining portions of the time courses plotted against a gray background. The colored lines are robust estimates of location (central tendency), whereas the error bars are robust standard errors (the scale estimate divided by the square root of the number of subjects) for each time point. The panels showing the results from the SLEA, NAc, hypothalamus (Hyp), GOb(5), and VT all show strong responses to the good spinner during the expectancy phase. In the SLEA and GOb(5), the peak responses increase monotonically with the expected value of the spinner, and in the NAc and hypothalamus, the responses to one or both of the lower value spinner are smaller than the responses to the good spinner. The remaining panel shows the time courses recorded in a left amygdala focus. In contrast to the pattern in the other five panels, there is little response to the good and intermediate spinners but a strong biphasic response to the bad spinner. The numbers under the name of each ROI reference the row numbers in Tables 1–4.

primary visual cortex activation (Tables S6 and S8 [see supplemental data]).

Behavioral and Questionnaire Data

During the prospect/expectancy phase of each trial, subjects made button-press responses identifying the currently projected spinner. The accuracy of performance on this task served as an index of vigilance. At the completion of scanning, a questionnaire was administered to assess the subjects' estimates of their cumulative gains and their experience of the prospects and outcomes.

Identification of Spinners and Tracking of Accumulated Gains

All subjects in the final cohort of 12 accurately identified the currently projected spinner. The average number of errors in the first run of 18 trials was 0.92 ± 0.33 (mean $\pm$ SEM); across the subsequent seven runs, the average number of errors per run ranged from 0.08 to 0.25. (These measures exclude responses on the "dummy trial" that led off each run.)

Only one of the 12 subjects reported that he was able to track his accumulated winnings throughout the imaging session. The actual winnings were $128.50 (the $50 endowment plus a total of $78.50 awarded during the scanning session); this subject estimated his winnings at $128. The estimates of two other subjects were 86% and 78% of the actual amount, whereas the next best estimate was only 47% of the total awarded; all the remaining subjects provided lower estimates. Thus, most of the subjects greatly underestimated their winnings (median estimate for all subjects = $50, interquartile range = $30) and do not appear to have kept track of their asset position.

Subjective Ratings of Prospects

Subjects rated the good spinner as a "better" prospect than the intermediate spinner, and the intermediate spinner as "better" than the bad spinner (Figure 7a). One-way ANOVA of these ratings indicates that the effect of spinner is highly reliable ($F[2, 33] = 56.93$, $p < 0.00005$). Subsequent pair-wise comparisons carried out by means of simultaneous 95% confidence intervals show that the ratings were reliably different and

were ordered according to the expected values of the spinners.

Subjective Ratings of Outcomes

In a two-way ANOVA of outcome ratings (with outcomes nested in spinners), the effect of outcome was highly significant (robust $F[6, 99] = 27.48$, $p < 0.00005$). Thus, the outcome ratings varied systematically as a function of the amount won or lost (Figure 7b). Contrasts based on simultaneous 95% confidence intervals around differences between the ratings of each of the extreme outcomes on a spinner and the middle outcome met the significance criterion in four of the six cases (*good spinner*: $2.50 versus $0; *intermediate spinner*: $2.50 versus $0, and $0 versus −$1.50; *bad spinner*: $0 versus −$1.50). The 95% simultaneous confidence intervals about the mean ratings of all positive outcomes are above zero, whereas the intervals about the mean ratings of all negative outcomes are below zero.

A $0 outcome appears on all three spinners. This outcome was rated highest when it appeared on the bad spinner and lowest when it appeared on the good. However, these differences are small and do not meet the criterion for statistical significance. Nonetheless, the simultaneous 95% confidence intervals about the mean rating of the zero outcome on the bad spinner does clear the baseline.

Discussion

Subjects witnessed a game of chance in which they won and lost money. On each play of the game, they were first shown their prospects, a set of three monetary values, and after a delay, they were shown how much they had won or lost. Subjects maintained a high and consistent level of vigilance as indicated by their low incidence of errors in identifying the currently displayed spinner. Most were unable to track their asset position and did not seem aware that their winnings grew over the course of the test session, suggesting that the baseline for evaluating the prospects and outcomes did not change systematically over trials.

Analysis of the functional imaging data reveals six principal findings. First, hemodynamic responses in the SLEA and GOb(5) tracked the expected values of the three spinners, and responses to good-spinner outcomes increased monotonically with monetary value in the NAc, SLEA, and hypothalamus. The orderings of these brain responses to prospects and outcomes parallel the post experiment ratings of prospect phase and outcome phase stimuli. Second, a broadly distributed set of brain regions was activated during the prospect phase, and responses in many of these regions were seen during the outcome phase as well; there was little evidence of anatomical segregation of prospect and outcome responses. Third, there was weak evidence for an influence of counterfactual comparisons on the BOLD response to the $0 outcome. Fourth, the hemodynamic responses in three dopamine terminal fields, the NAc, SLEA, and hypothalamus, show intriguing parallels to electrophysiological recordings from VT dopamine neurons obtained in monkeys during anticipation and experience of rewards. Fifth, the results are suggestive of a hemispheric bias in the processing of expectancies,

and perhaps outcomes as well. The predominant responses to gains or their prospects were noted in the right hemisphere, whereas left hemisphere activations predominated in response to negative prospects. Lastly, an incentive unique to humans, money, produced hemodynamic activations overlapping those seen previously in response to tactile stimuli, gustatory stimuli, and euphoria-inducing drugs. This overlap is consistent with the involvement of common, generalized circuitry in the processing of different categories of rewards.

Ordering of fMRI Signals

Prospect Responses

Hemodynamic responses to prospects in the SLEA and GOb(5) track the expected values of the spinners (Figure 3). A tendency toward such orderings was observed in the NAc and hypothalamus, where responses to one or both higher-valued spinners exceeded the responses to one or both lower-valued spinners. In contrast, the response to the negative prospect predominated in the left amygdala. The ordering of prospect responses in these ROIs should be considered in the context of two overall groupings: eight regions where responses to positive prospects predominated and four regions where only the prospect responses to the bad spinner cleared the baseline (Tables 1 and 2; Figure 3). The responses in these two groupings would appear to provide adequate information to account for the subjective reports of spinner impact (Figure 7a), i.e., an observer could generate orderly and realistic prospect ratings based on the fMRI time courses alone.

Fewer than half as many clusters showed a dominance of responses to the bad prospects than to the good. Although losses tend to loom larger than gains of equal magnitude (Kahneman and Tversky, 1979), it is possible that the disparity between the values employed in this study was too large. It is also possible that the $50 endowment and the knowledge that the subject could suffer no real net loss diminished the impact of the bad spinner.

Outcome Responses

A main effect of outcome was seen in the ANOVA of the time courses from 11 ROIs. Given these differential responses, the changes in the recorded signal during the outcome phase cannot have been due simply to the waning of the response to the preceding prospect display, which was the same for each outcome on a given spinner.

The most sustained outcome phase responses were recorded in the NAc, SLEA, hypothalamus, and VT; in the NAc, SLEA, and hypothalamus, the responses to the outcomes on the good spinner were ordered as a function of monetary payoff (Figure 4a). These orderings of brain responses to good-spinner outcomes parallel the ordering of the subjective ratings (Figure 7b). In contrast, the ordering of responses in some ROI-based foci differed from the ordering of the subjective ratings. For example, the responses in cluster GOb(4) to the two most extreme outcomes ($10, −$6) are the only ones to reliably clear the baseline (Figure 4b). These responses provide information about the magnitude of the outcomes but not their sign. Activation of a GOb focus reflecting the magnitude of cumulative monetary win-
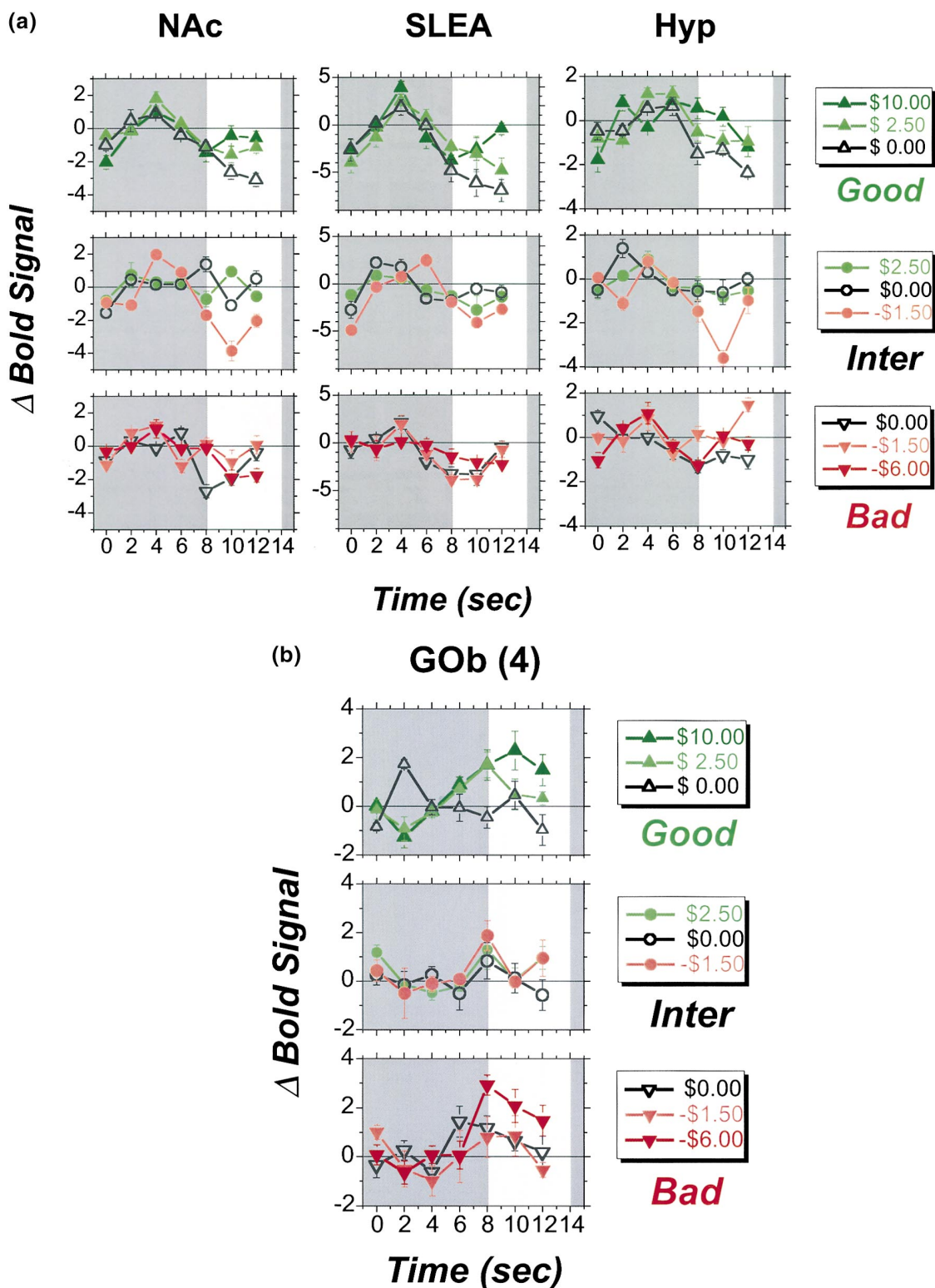
Figure 4. Outcome Phase Time Courses

Robust time courses illustrating outcome phase responses in four ROIs are shown, using the same color coding to designate trial types as in Figure 1b. Time courses for good-spinner, intermediate-spinner, and bad-spinner outcomes are shown in the top, middle, and bottom rows of graphs, respectively. The white background highlights the time window employed in the analysis of outcome phase responses, and the remaining portions of the time courses are plotted against a gray background. The 8 s of data acquired before the outcome phase of the experiment were used to zero the data (see Figure S5 [see supplemental data at http://www.neuron.org/cgi/content/full/30/2/619/DC1]). The three columns of data from the NAc, SLEA, and hypothalamus (Hyp) in (a) are grouped to illustrate regions that show differential responses

Table 3. ANOVA: Prospect/Expectancy Pair-Wise Comparison

Anatomy	Time Point and Valence of Comparison		
	G vs. I	I vs. B	G vs. B
Frontal Lobe			
GOb(1) (L)	—	6 (−)	6 (−)
GOb(10) (L)	—	5, 6, 7 (−)	—
Temporal Lobe			
Medial			
Amygdala(11) (L)	—	7 (−)	—
Subcortical Gray			
NAc(13) (R)	—	7 +	—
SLEA(14) (R)	—	7 +	6, 7 +
Hypothalamus(15) (R)	7 +	—	7 +

Table 3 summarizes the results of pair-wise comparisons performed if the spinner or spinner * time point conditions were significant in the robust ANOVA of expectancy phase responses, as listed in Table 1. ROI# follows the numbering established in Table 1. Pair-wise comparisons are listed for the following contrasts: good versus intermediate, intermediate versus bad, and good versus bad spinners. If a comparison is significant, it is listed by the time point when it is observed, and its valence is also noted by + or −. If it is not significant, then a dash is listed.

nings, but not their sign, has been reported by Elliott et al. (2000).

The design of the experiment made it possible to determine qualitatively whether, as predicted by decision affect theory (Mellers et al., 1997), responses to a given outcome depend on counterfactual comparisons. There is a suggestion of such an effect in the functional imaging data. The work of Mellers et al. (1997) predicts that the $0 outcome on the good spinner will be experienced as a loss, whereas on the bad spinner, it will be experienced as a win. As shown in Figure 5, the responses in the NAc and SLEA to the $0 outcome on the good spinner drop below the time courses for the $0 outcomes on the other spinners, whereas the responses to the $0 outcome on the bad spinner climb above the responses to the $0 outcome on the good spinner (like the responses in the NAc and SLEA to the $10 outcome on the good spinner). These differences cannot be due to the normalization to the prospect phase median because the signals change over time during the outcome phase.

Although the time courses for the $0 outcome on the good and bad spinners are consistent with the notion that counterfactual comparisons are reflected in the BOLD signals, the time courses for the $0 outcome on the intermediate spinner do not lie, as predicted, in between the other two time courses. Thus, support for counterfactual comparison is equivocal. Interposition of a delay between the prospect and outcome display might yield cleaner results by eliminating the overlap of the later portion of the prospect response and the early portion of the outcome response.

Procedural differences may explain why clear evidence for a dependence of subjective ratings on counterfactual comparisons was obtained by Mellers et al. (1997), whereas no reliable effect was seen in the subjective outcome ratings reported here (Figure 7b). The ratings in the study by Mellers and colleagues (1997) were performed on a trial-by-trial basis, immediately after each outcome was revealed. In contrast, the subjective ratings reported here were obtained only at the end of the entire session, when the experience of the different outcomes was no longer so vivid in memory, and hence the ratings may well have been dominated by the objective monetary amounts.

Interrelationship of Expectancy Phase and Outcome Phase Time Courses

There was little tendency for prospect phase responses to be restricted to one set of clusters and outcome phase responses to another. That the results of the time course analysis are less segregated by trial phase than the results of initial cluster selection procedure is consistent with the greater specificity and sensitivity of the normalization and robust estimation methods employed in the time course analysis.

The work of Mellers et al. (1999, 1997) suggests a simple interpretation of the tendency for prospect phase and outcome phase responses to be seen in the same brain regions. In this view, a subject observing one of the spinners during the prospect phase would compute an expected emotional response to the outcome on each sector and then perform a combinatorial operation, such as averaging, to obtain an expected emotional response to the prospect represented by the spinner as a whole. Once the arrow stopped rotating and the outcome was revealed, the subject would again compute an emotional response to the gain or loss. If, as Mellers et al. (1999) propose, common psychological mechanisms are used to compute expectancies and to evaluate outcomes, then it would stand to reason that common neural circuitry were employed.

Alternatively, different neural substrates may encode prospect phase and outcome phase information, but the components of this circuitry may be segregated anatomically on a spatial scale finer than our imaging system can resolve. If such neural substrates were proximate to each other, as has been suggested for regions evaluating the anticipation and experience of painful stimulation (Ploghaus et al., 1999), they would appear colocalized.

It is important to note that colocalization and coordination of prospect phase and outcome phase responses was not seen in all clusters. For example, a clear exception to this pattern was seen in GOb(4), where outcome phase responses were recorded in the absence of systematic prospect phase responses (Figure 4b). Such

to the outcomes on the good spinner. Note that the magnitude of these good-spinner outcome phase responses increases monotonically as a function of the monetary value of the outcome. Similar orderings are not observed for outcomes on the intermediate or bad spinners, although the time courses for the lowest valued outcome on the intermediate spinners fall below the others. The ROI in (b), GOb(4), illustrates a very different profile of outcome responses to the monotonic ordering seen in the top row of (a). Time courses from this ROI appear to respond to the magnitude, but not the sign, of the outcomes. Strong positive responses are seen to the two extreme outcomes: +$10 and −$6.
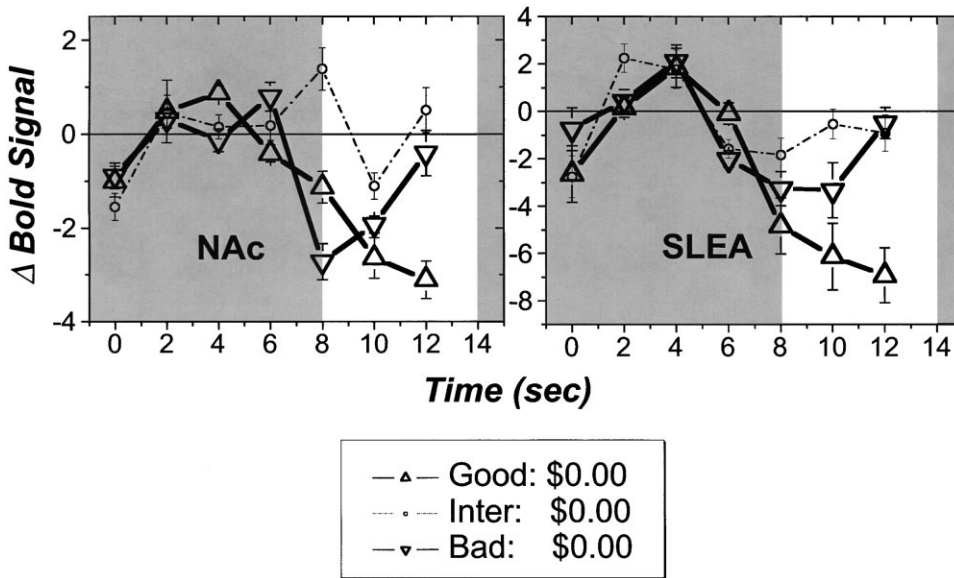
Figure 5. Time Courses for the $0 Outcome

These fMRI time courses from the NAc and SLEA show responses to the $0 outcome on each of the three spinners. As in Figures 4a and 4b, the prestimulus baseline from the 8 s preceding the outcome phase of the experiment was used to zero the outcome data, and the time window employed in the analysis of the outcome responses is highlighted by a white background. These data are presented to illustrate the putative influence of prior expectancy and counterfactual comparison on the outcome phase data. The $0 outcome on the good spinner is the worst of the three outcomes available on that spinner, and the corresponding time course in each of these ROIs declines during the outcome phase. In contrast, the $0 outcome on the bad spinner is the best of the three available outcomes, and the corresponding time courses either remain stable or climb during the outcome phase.

results hint at diversity in the way that prospects and outcomes are processed in different brain regions.

Functional Imaging and the Psychology of Judgment and Decision

In prior functional imaging studies, responses to monetary gains and losses or to winning and losing game points have been noted in a subset of the regions targeted in this study (Breiter et al., 1996b; Elliott et al., 2000; Knutson et al., 2000; O'Doherty et al., 2001; Rogers et al., 1999; Thut et al., 1997). A broader distribution of activations may have been observed in the present study due to the incorporation of basic principles derived from the psychological study of judgment and decision and the application of robust statistical methods.
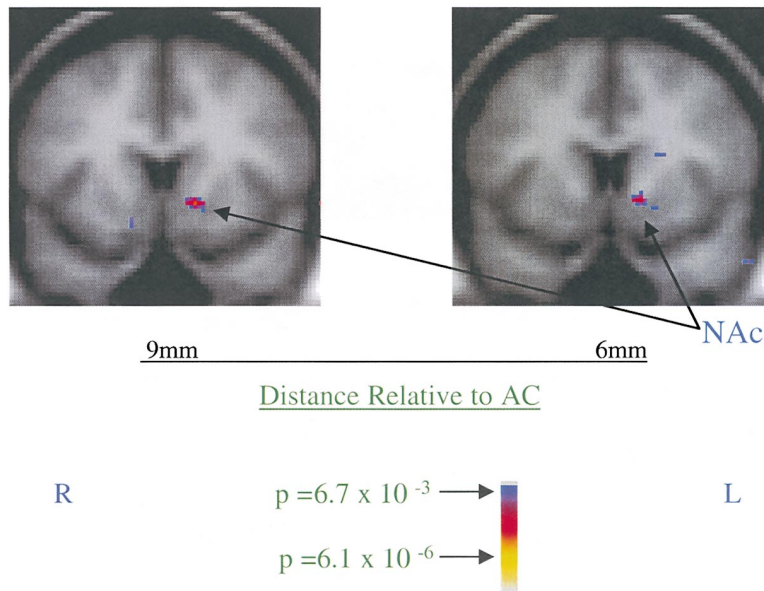
As suggested by decision affect theory (Mellers et al., 1997), the experiment was designed so as to control, manipulate, and asses the influence of prior expecta-

Table 4. ANOVA: Outcome Pair-Wise Comparisons

Anatomy	Good Spinner			Intermediate Spinner			Bad Spinner		
	High vs. Median	Median vs. Low	High vs. Low	High vs. Median	Median vs. Low	High vs. Low	High vs. Median	Median vs. Low	High vs. Low
Frontal Lobe									
GOb(1) (L)	—	—	—	—	—	—	9 +	—	—
GOb(5) (R)	—	8 (−)	—	—	9 (−)	—	—	—	—
GOb(6) (R)	—	—	—	8 (−)	—	—	—	8 +	—
GOb(10) (L)	—	8 +	—	—	—	—	—	—	8 (−)
Temporal Lobe Medial									
Amygdala(11) (L)	—	8 (−)	—	—	—	—	—	—	—
Amygdala(12) (R)	—	—	—	—	—	—	—	—	9 +
Subcortical Gray									
NAc(13) (R)	—	10 +	9, 10 +	8 (−), 9 +	9, 10 +	9 +	8 (−)	—	8 (−)
SLEA(14) (R)	—	—	10 +	—	9 +	—	—	—	—
Hypothalamus(15) (R)	—	—	8 +	—	9 +	9 +	—	—	—

Table 4 summarizes the results of pair-wise comparisons performed if the main effect of trial type or the trial type * time point interaction was significant in the robust ANOVA of outcome phase responses, as listed in Table 1. ROI# is consistent with the numbering established in Table 1. Three separate comparisons are listed for each spinner; the highest monetary outcome with the median outcome, the median outcome with the lowest outcome, and the highest outcome with the lowest outcome. If a comparison is significant, it is listed by the time point where it is observed, and its valence is also noted by + or −. If it is not significant, then a dash is listed.

Positive fMRI Signal Change in the NAc During Expectancy of Monetary Gain

R   p =6.7 x 10^{-3} ⟶

                     p =6.1 x 10^{-6} ⟶   L

Distance Relative to AC

9mm   6mm   NAc

Figure 6. Prospect Phase Response in the NAc

Significant NAc signal change is illustrated for the voxel-by-voxel correlational analysis performed post-hoc. Gray-tone averaged structural MRI images for the 12 subjects underlie pseudocolor p value maps for correlation of the difference signal against the simulated γ function. Note that left NAc activation is observed for this post-hoc comparison solely for the good to intermediate spinner comparison, in contrast to the right NAc activation observed in the ROI-based analysis, for which multiple expectancy and outcome effects were noted.

tions and counterfactual comparisons. Trials were structured so as to separate the onset of prospect and outcome responses in time. As suggested by prospect theory (Kahneman and Tversky, 1979), cumulative winnings were not displayed, thus increasing the likelihood that performance on each trial would be referenced to a common baseline. Additional features of the design made it possible to determine how the BOLD signal varied as a function of the magnitude and sign of the outcomes. Only a few of these features are shared with prior functional imaging studies of the anticipation and/or experience of monetary or token gains and losses (Breiter et al., 1996b; Elliott et al., 2000; Knutson et al., 2000; O'Doherty et al., 2001; Rogers et al., 1999; Thut et al., 1997).

Evidence Linking the Regions of Interest to the Anticipation and Experience of Positive and Negative Outcomes
Hemodynamic responses to tactile stimuli, gustatory stimuli, or euphoria-inducing drugs have been reported

in subsets of the six regions targeted by this study (Breiter et al., 1997; Stein et al., 1998; Breiter et al., 1998; Zald et al., 1998; Francis et al., 1999; Breiter et al., 2000; Small et al., 2001). In the sections that follow, selected findings from studies of humans and laboratory animals are reviewed, linking each of these target regions to anticipation and the experience of gains and losses.
VT Dopaminergic Neurons
There are striking resemblances between the BOLD time courses recorded from the NAc, SLEA, hypothalamus, and VT and electrophysiological recordings obtained by Schultz and coworkers from single dopaminergic VT neurons (Schultz, 1986; Schultz et al., 1997; Schultz and Romo, 1990). These resemblances are of particular interest given that dopaminergic VT neurons project to the NAc, SLEA, and hypothalamus (Heimer et al., 1997; Lindvall and Bjorklund, 1974; Lynd-Balta and Haber, 1994) and that cocaine-induced enhancement of dopaminergic action increases the BOLD signal in the NAc and SLEA terminal fields (Breiter et al., 1997).

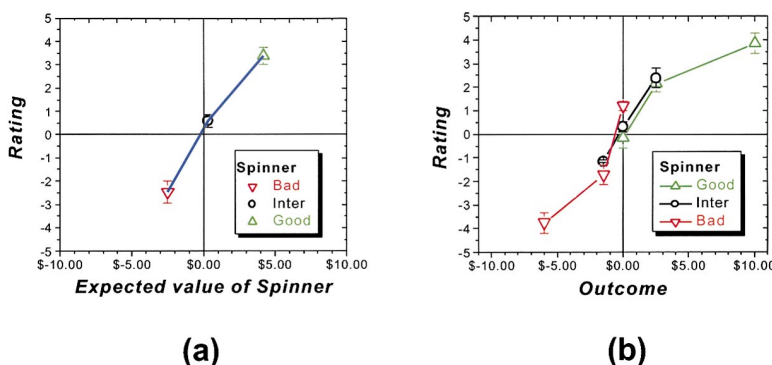Dopamine neurons in the VT fire in response to re-

(a)   (b)

Figure 7. Subjective Ratings of Spinners and Outcomes

Subjective ratings of spinners (a) and outcomes (b). At the very end of the experiment, subjects marked on an 11-point opponent scale (range –5 to 5) their remembered subjective experience of each spinner and each outcome. The data points are robust medians, and the error bars are mean deviations from the median (MAD). These ratings are graphed relative to the mean monetary value (i.e., expected value) of each spinner (Figure 2a) and outcome (Figure 2b).

ward-predicting stimuli, paralleling the increases in fMRI signal reported here in response to the good spinner in the NAc, SLEA, hypothalamus, VT, and some GOb clusters (Figure 3). There are also similarities between the BOLD responses to outcomes in the NAc, SLEA, and hypothalamus (Figure 4a) and the neuronal firing changes described by Schultz and coworkers in response to reward presentation or omission. Firing increases in dopaminergic VT neurons in response to better-than-expected outcomes. Similarly, the BOLD signal in the NAc, SLEA, and hypothalamic terminal fields was highest in response to the better-than-average outcome and lowest in response to the worse-than-average outcome on the good spinner. The lack of systematic responses to the outcomes on the bad spinner may be related to the lack of responsiveness to mild aversive stimuli noted by Mirenowicz and Schultz (1996), although strong aversive stimuli are known to activate VT dopaminergic neurons (Guarraci and Kapp, 1999; Horvitz, 2000).

In contrast to the responses in the NAc, SLEA, and hypothalamic terminal fields, the fMRI signals in the VT itself were not graded as a function of spinner. This lack of gradation of signals from VT does not fit simply into the framework proposed by Schultz and his coworkers but is not necessarily incompatible with it. Montague et al. (1996) along with Schultz et al. (1997) interpret the dopaminergic response to rewards as a prediction error, a signal that reflects the difference between expectation and outcome. Their adaptation of the temporal-difference model of reinforcement learning (Sutton and Barto, 1998) predicts that the magnitude of the anticipatory burst is proportional to the magnitude of the reward. Thus, a negative prospect would not be expected to activate dopamine terminal fields. Nonetheless, it is conceivable that the observed expectancy responses reflect only the positive components of the prospects offered by a given spinner (e.g., the $0 outcome on the bad spinner). Our results might also be viewed in terms of (a) the alternative proposal of Redgrave et al. (1999a, 1999b) that the anticipatory burst of dopaminergic firing is tied to the switching of behavioral and attentional resources, or (b) the formulations of Blackburn and colleagues (1992) and Horvitz (2000) that dopaminergic neurons respond to motivationally significant and/or arousing environmental changes.

NAc

Increases in NAc dopamine release in anticipation of reward delivery (Pfaus et al., 1990; Richardson and Gratton, 1996), firing of local cell bodies, and nondopaminergic inputs (Carlezon and Wise, 1996; Hauber et al., 2000) may have contributed to the responses observed in the NAc. Ventral striatal neurons in monkeys show increased activity in anticipation of and following reward delivery (Hollerman et al., 1998; Schultz et al., 1992; Tremblay and Schultz, 1999). Activation of the human NAc in anticipation of a reward (i.e., a potential cocaine infusion) has also been observed (Breiter and Rosen, 1999). Breiter and Rosen (1999) have argued that activation of the NAc in this study and others (Berns et al., 1997) can best be understood in terms of the evaluation of probabilistic contingencies.

SLEA

The prospect and outcome responses in the SLEA parallel results from Wilson and Rolls (1990), showing that neurons in the monkey SLEA fire in response to stimuli signaling the availability of a palatable liquid, as well as during delivery of this reward. Neurons in the SLEA are activated by rewarding brain stimulation in the rat (Arvanitogiannis et al., 1996, 2000; Flores et al., 1997; Nakahara et al., 1999; Shizgal, 1997). Lesions of the SLEA reduce the rewarding effect of medial forebrain bundle stimulation (Arvanitogiannis et al., 1996), reduce self-administration of cocaine (Robledo and Koob, 1993), and disrupt operant performance for sucrose pellets in rats (Brown et al., 1996). Recent evidence suggests that the SLEA may also respond to nonrewarding stimuli: transient activation in this region has been reported following painful cutaneous stimulation in humans (Becerra et al., 2000; Borsook et al., 2000).

Hypothalamus

The evidence linking hypothalamic neurons to positive prospects and outcomes includes single-neuron recordings in awake monkeys (Rolls et al., 1976; Scott et al., 1995) and rats (Ono et al., 1986), increases in immediate-early gene expression in response to rewarding brain stimulation in rats (Arvanitogiannis et al., 1996, 2000; Flores et al., 1997; Nakahara et al., 1999), and attenuation of brain stimulation reward by excitotoxic lesions (Arvanitogiannis et al., 1996).

Amygdala

A vast literature links the amygdaloid nuclei to the processing of the motivational significance of stimuli and to the control of emotion (Davis, 1992; Everitt et al., 1991; Everitt and Robbins, 1992; Kapp et al., 1992; LeDoux, 1992, 1996). Of particular relevance are single-unit recordings showing changes in the firing of basolateral amygdala neurons in anticipation of both positive and negative outcomes in rats (Schoenbaum et al., 1998, 2000) and in monkeys (Rolls, 1999). In the sense that fear entails anticipation of a negative outcome, data linking amygdaloid neurons to fear conditioning (Davis, 1992; LeDoux, 1992, 1994, 1995, 1996; Quirk et al., 1995) is also germane. In this regard, activation of the left amygdala has been consistently reported in response to fearful faces in multiple neuroimaging studies (Breiter et al., 1996a; Morris et al., 1996; Phillips et al., 1999; Thomas et al., 2001).

GOb

GOb neurons in the rat (Schoenbaum et al., 1998, 1999) and the monkey (Rolls, 2000; Tremblay and Schultz, 1999) have been observed to fire during the anticipation and experience of positive and negative outcomes. Responses of GOb neurons may be tuned to particular sensory modalities or conjunctions of modalities (Rolls, 2000), reflect the waning of reward during satiation (Rolls et al., 1989), and represent relative reward preferences (Tremblay and Schultz, 1999). The richness and variety of the tuning characteristics of GOb neurons may account for the diverse patterns of GOb prospect and outcome responses observed in the present study.

Other Brain Regions Associated with the Anticipation and Experience of Positive and Negative Outcomes

Post-hoc signal changes were noted in the lateral prefrontal cortex and the lateral temporal cortex. These regions have been interpreted to constitute part of a distributed system for expectancy evaluation (Breiter and Rosen, 1999). The lateral prefrontal cortex activations parallel observations by Watanabe (1996) that lat-
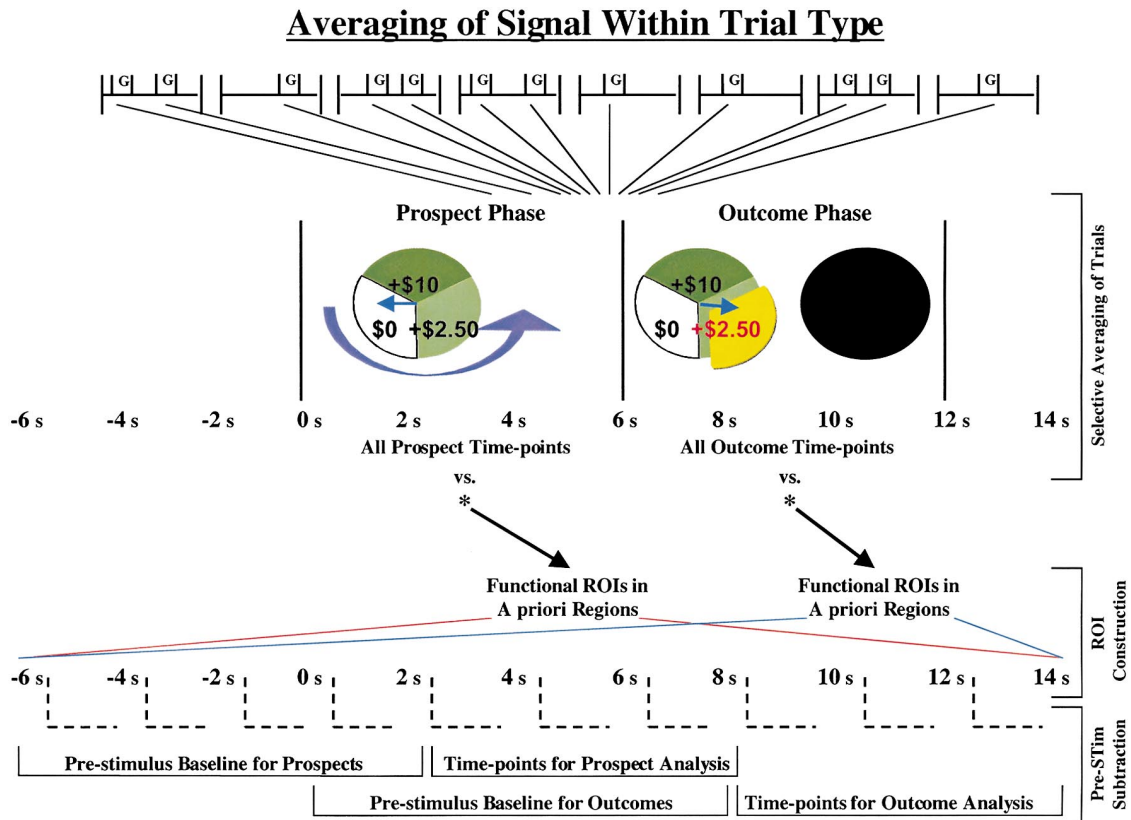
Averaging of Signal Within Trial Type

Figure 8. The General Schema for the Single Trial Analysis

The general schema for the single-trial analysis. 20 s time courses for each trial were selectively averaged within individual; these included the three time points preceding the onset of each trial as well as the time point immediately following trial offset. The time points constituting the prestimulus baseline for the prospect phase the outcome phase time courses are shown at the bottom.

eral prefrontal neurons fire in response to the expectancy of a specific reward and are important for monitoring the context in which the reward is experienced. These findings are noted to emphasize the likelihood that brain regions in addition to those targeted in this study may play a role in the experience of gains and losses.

Hemispheric Specialization

Reliable deviations of expectancy phase time courses from baseline can be subdivided into two categories. The first includes eight right-hemisphere ROIs where positive-going prospect phase responses were seen in response to the good spinner and often to the intermediate and bad spinners as well. In contrast, signals in a set of left-hemisphere ROIs deviate reliably from baseline only in response to the bad spinner. The post-hoc voxel-by-voxel correlational analysis does provide some counterexamples, such as responses to positive prospects and outcomes in the NAc and GOb. Nonetheless, the rather consistent asymmetry of the ROI-based results, particularly in the case of the subcortical structures, suggests a hemispheric bias in the processing of positive and negative expectancies.

The hemispheric bias in the results of the time course analysis contrasts with current ideas about hemisphere specialization in the processing of positive and negative emotions, such as the approach-withdrawal model of

cerebral asymmetry (Davidson, 1998; Davidson and Sutton, 1995; Sutton and Davidson, 1997). In this view, processing in the left prefrontal cortex is linked to positive affect and processing in the right prefrontal cortex with negative affect. The time scale of these emotional responses is both short term (e.g., induced emotion) and long term (e.g., depression and brain damage). In contrast, the current study emphasized a very short-term time scale (6 s per trial phase). Temporal differences in testing paradigms and spatial differences in regions targeted may have contributed to the contrast between the results reported here and those that compose the basis for theories such as the approach-withdrawal model of cerebral asymmetry. In this regard, it is interesting to note the parallel between the current data from the left amygdala and previously reported responses to fearful facial expressions in subcortical regions of the left hemisphere (Breiter et al., 1996a; Morris et al., 1996; Phillips et al., 1999; Thomas et al., 2001).

Limitations

A number of limitations apply to this fMRI study, which have been discussed at length in prior manuscripts (Breiter et al., 1996a, 1996c, 1997). These issues include the limited signal-to-noise ratios of BOLD signals recorded from small subcortical structures, spatial resolution after data analysis, magnetic susceptibility, and un-

certainty concerning how fMRI signals are linked to underlying neuronal activity.

The confirmation of the initial cluster selection by the time course analysis in 15 of 16 cases shows that the initial screening entailed little Type II error. Type I errors would be expected in the case of opponent responses to different trial types, which would tend to cancel as a result of averaging, or responses confined to a small proportion of trial types, which would tend to be diluted by averaging. Noteworthy in this regard is the left NAc signal change observed by the post-hoc voxel-by-voxel correlational analysis that was not picked up by the cluster selection method.

The primary transformations performed on these data involved motion correction, spatial transformation into a uniform anatomic space, and smoothing of the statistical maps for cluster analysis. As discussed in detail in the addendum on http://www.neuron.org/cgi/content/full/30/2/619/DC1, the estimated effective spatial resolution after data analysis (Fischl et al., 1999) is 6.9 mm, which is well within the spatial scale required to localize the NAc, SLEA, amygdala, and VT (Makris et al., 1999).

Given this study was performed on a 3 T magnet, susceptibility effects around target structures were a significant concern. To minimize such effects, we utilized a shimming routine with second order shims. The resultant radio-frequency line-widths were all minimized with low variance across subjects. To further reduce susceptibility effects, voxels used for data acquisition were nearly isotropic, thus reducing within slice dephasing of spins and loss of magnetization. A short echo time (TE) further helped minimize spin dephasing. Lastly, activations were evaluated using an objective method (Breiter et al., 1997) to determine that they did not overlie regions of potential susceptibility represented by signal drop-off.

Conclusions

The results of this experiment coupled with findings from prior studies of the anticipation and experience of positive and negative outcomes in humans and laboratory animals suggest that a network of interrelated structures at different levels of the neuraxis coordinate the processing of goal-related stimuli. A challenge for future work is to determine the roles played by the different components of this circuitry in the cognitive, emotional, and motivational processes involved in anticipation, evaluation, and decision making. Experimental paradigms incorporating psychological principles derived from the study of judgment and decision should prove important to the success of this endeavor.

The psychological processes underlying the anticipation and experience of monetary prospects and outcomes would appear to play an important role in gambling and in other behaviors that entail decision making under uncertainty. In this regard, it is striking that the activations seen in the NAc, SLEA, VT, and GOb in response to monetary prospects and outcomes overlap those observed in response to cocaine infusions in subjects addicted to cocaine (Breiter et al., 1997) and to low doses of morphine in drug-naïve individuals (Breiter et al., 2000). These common patterns of hemodynamic response are consistent with the view that dysfunction of neural mechanisms and psychological processes crucial to adaptive decision making and behavior may contribute to a broad range of impulse disorders such as drug abuse and compulsive gambling.

Experimental Procedures

Subjects

Twenty right-handed male subjects were recruited for this experiment. Due to uncorrectable motion or spiking artifact, functional imaging data from eight subjects could not be used. All subjects were deemed medically, neurologically, and psychologically normal by self-report and physician-directed medical review of systems. No subject had a history of head trauma with loss of consciousness for more than 30 s nor a history of surgery with general anesthesia or pain medication. The average age of the 12 subjects with motion correctable data was 27.3 ± 1.32 years (mean ± SEM). Their scores on the Beck Depression Inventory (range 0–63) and Beck Anxiety Inventory (range 0–63) were 3.3 ± 0.93 and 2.7 ± 0.70, respectively (mean ± SEM). All subjects gave informed consent to participate in these procedures following the rules of the Subcommittee on Human Studies at the Massachusetts General Hospital.

Experimental Design

Subjects viewed stimuli projected onto a mirror within the bore of the magnet. The display consisted of either a fixation point or one of three disks ("spinners"). Each spinner (Figures 1a and 1b) was divided into three equal sectors. The "good" spinner could yield either a large gain (deep green sector, labeled: +$10), a small gain (light green sector, labeled +$2.50), or no gain (white sector, labeled $0), the "bad" spinner could yield a large loss (deep red sector: −$6), a smaller loss (light red sector: −$1.50), or no loss (white sector: $0), and the "intermediate" spinner could yield a small gain (light green sector: +$2.50), a small loss (light red sector: −$1.50), or neither a loss nor a gain (white sector: $0). The gains were made larger than the losses to compensate for the well-established tendency of subjects to assign greater weight to a loss than to a gain of equal magnitude (Kahneman and Tversky, 1979).

Before the game began, subjects were shown each spinner three times so as to learn its composition. Each trial consisted of (1) a "prospect phase," when a spinner was presented and a superimposed arrow spun around its center, and (2) an "outcome" phase, when the arrow landed on one sector and the corresponding amount was added to or subtracted from the subject's winnings (see Figure 1a). During the prospect phase, the image of one of the three spinners was projected for 6 s, and the subject pressed one of three buttons to identify the currently displayed spinner (or fixation point), thus providing a measure of vigilance. The display was static for the first 0.5 s, and then a superimposed arrow began to rotate. The arrow came to a halt at 6 s, marking the end of the prospect phase. During the first 5.5 s of the ensuing outcome phase, the sector where the arrow had come to rest flashed, indicating the outcome. A black disk was then projected as a visual mask during the last 0.5 s of the 12 s trial. On fixation point trials, an asterisk appeared in the center of the display for 15.5 s, followed by the 0.5 s mask.

The pseudorandom trial sequence was fully counterbalanced so that trials of a given type (spinner + outcome) were both preceded and followed once by all nine spinner/outcome combinations and three times by fixation point trials. Thus, the average one-trial "history" and "future" were the same for trials of every type. The trial sequence was subdivided into eight runs of 19 trials, separated by 2–4 min rest periods. The initial trial (i.e., "dummy trial") in each run served only to maintain counterbalancing, and functional imaging data were not obtained during this trial. The same trial sequence was used for all subjects, generating winnings of $78.50; to which was added the $50 endowment.

Subject Instructions

By reading a set text, subjects learned that they would be participating in a game of chance. At the start of this game, they were awarded an endowment of $50 to cover possible losses and informed of the maximum they could win over the course of the experiment. Subjects were told that in the unlikely event they lost more than their

endowment, they would receive no money, but they would be given a picture of their brain in action and have a clinical scan on record, worth approximately $1600. The spinners and the trial structure were then described. The subjects were instructed to identify each spinner as rapidly as possible using the button box and to refrain from speech during the scan. After reading the instruction text, subjects' questions were answered, and they then observed a sample set of ten trials, including all trial types, to familiarize them with the stimuli.

Behavioral Monitoring

Throughout the scanning session, subjects identified the currently presented spinner using designated keys on a button box. They were instructed to make no responses during fixation point epochs. Button box responses were transmitted as ASCII data to a Macintosh computer.

Imaging

Subjects were scanned on an instascan device (3 T General Electric Signa; modified by Advanced NMR Systems, Wilmington, MA) using a GE head coil. Imaging for all experiments started with a sagittal localizer scan (conventional T1-weighted spoiled gradient refocused gradient echo [SPGR] sequence; through-plane resolution = 2.8 mm; 60 slices) to orient, for subsequent scans, the slices to be acquired for functional scanning. This scan was also used as the structural scan for Talairach transformation. Next, an automated shimming technique was used to optimize B_0 homogeneity (Reese et al., 1995). Radio frequency full-width half-maximum (FWHM) line-width after shimming of primary and secondary shims produced a measure of 32.4 ± 2.2 for the 12 subjects with motion-correctable functional data. After shimming, experimental slices were pre-scribed, with 18 slices parallel to the AC-PC line and covering the NAc, amygdala, SLEA, and VT. In this orientation, an SPGR T1-weighted flow-compensated scan was obtained (resolution = 1.6 mm $\times$ 1.6 mm $\times$ 3 mm), primarily to aid Talairach transformation during data analysis (Breiter et al., 1996a, 1996c). The fourth scan was a T1-weighted echo planar inversion recovery sequence (TI = 1200 ms, in-plane resolution = 1.57 mm) for high-resolution structural images to be used in preliminary statistical maps (but not with Talairach transformed or averaged maps). Finally, functional scans employed a T2*-weighted gradient echo sequence (TR = 2 s, TE = 35 ms; Flip = 70°; in plane resolution = 3.1 $\times$ 3.1 mm, through-plane resolution = 3 mm, FOV = 40 $\times$ 20 cm; 18 contiguous slices, images per slice = 108 per run with ten disdaq for each of the eight runs).

Post Scan Interview

Following the scanning session, the subjects completed a questionnaire that assessed their ability to track their cumulative winnings/losses during the experiment and asked for estimates of total winnings as well as ratings of the subjective impact of each spinner and outcome. The ratings were registered as a mark on an 11-point, opponent scale ranging from very bad (−5) to very good (+5). Subjects were informed subsequently of their total gains from the experiment.

Data Analysis

A statistical expert system (RS/Explore, Brooks Automation), was used to compute descriptive statistics and to carry out hypothesis testing. Exploratory data analysis revealed that the across-subject distribution of scores was contaminated by extreme values in some data sets, thus deviating substantially from normality. Robust statistics based on the Tukey bisquare estimator (Hoaglin et al., 1983) were used when the presence of such extreme values ("outliers") was detected by the expert system. Such statistics are less subject than conventional parametric statistics to the influence of outliers and provide more efficient estimates of the central tendency ("location") and dispersion ("scale") of contaminated normal distributions. Although robust methods are more efficient when dealing with contaminated distributions, they are less efficient than parametric statistics when dealing with near-normal distributions. Thus, the expert system recommends the use of the robust methods only when the efficiency of such methods is greater than the efficiency of conven-

tional parametric ones. Similarly, the expert system recommends the use of variance-adjusted weights only when the dispersion of scores varies substantially across groups. The recommendations of the expert system were followed in all cases. A description of the robust extimators, the test for relative efficiency of the robust and parametric estimators, and the test for unequal dispersion of scores across groups is provided in an appendix available (see supplemental data at http://www.neuron.org/cgi/content/full/30/2/619/DC1).

Behavioral Data

The identification of the currently projected spinner by the 12 subjects with motion-correctable functional data was checked against the trial sequence. The mean number of errors and the standard error of the mean (SEM) were computed for the last 18 trials of each of the eight runs.

Post Scan Interview Data

The ratings of prospects and outcomes by the subjects with motion-correctable functional data were tabulated and evaluated using the expert statistical system to carry out ANOVAs and subsequent contrasts. Planned pair-wise comparisons of the ratings of the good and intermediate spinners and the bad and intermediate spinners were carried out, based on simultaneous confidence intervals. When this type of confidence interval is used, the statistical threshold is adjusted as a function of the number of possible pair-wise comparisons, thus defending the α level.

The two-way ANOVA of outcome ratings was structured so that outcomes were nested within spinners. Six planned post-hoc comparisons were carried out: the ratings of the two extreme outcomes on each of the three spinners were compared to the ratings of the middle outcome. These comparisons were based on simultaneous confidence intervals.

FMRI Data

Transformation of fMRI BOLD Data before Statistical Mapping

Motion Correction. A bite-bar was employed to reduce head motion, and BOLD data were motion corrected using an adapted algorithm (Jiang et al., 1995; Woods et al., 1992; Breiter et al., 1996c). After motion correction, time series data were inspected to ensure that no data set evidenced residual motion in the form of cortical rim or ventricular artifacts > 1 voxel. From this analysis, 8 of 20 subjects were found to have uncorrectable motion or spiking artifact. In the remaining subjects, motion correction (mean $\pm$ SEM) of the BOLD data revealed a range of average maximal displacements for each of the eight runs of 0.43 ± 0.097 mm to 1.47 ± 0.43 mm. Motion displacement led to a range of corrections for movement, in terms of the mean correction per time point for each of these runs, of 0.22 ± 0.04 mm to 1.29 ± 0.41 mm.

Signal Normalization and Filtering. For all eight runs, fMRI data in the Talairach domain were intensity scaled on a voxel-by-voxel basis to a standard value of 1000, so that all mean baseline raw magnetic resonance signals were equal. These data were then de-trended to remove any linear drift over the course of the scan. Spatial filtering was performed using a Hanning filter with 1.5 voxel radius (this approximates a 0.7 voxel gaussian filter). Lastly, the mean signal intensity for each voxel over all runs was removed on a time point by time point basis.

Averaging of Signal Time Courses within Subjects. The rationale for the averaging of time courses and their subsequent analysis is based on two assumptions: (a) that the behavior of the hemodynamic control system is approximately linear (i.e., it obeys the superposition axiom) under the experimental conditions tested and in the brain regions targeted by this experiment, and (b) that deviations from hemodynamic stationarity were correctable by means of the normalization procedures employed. If the hemodynamic control system obeyed superposition and stationarity, then the counterbalancing procedure ensured that any carryover of hemodynamic responses from the antecedent trial was constant across trial types.

In total, there were ten trial types (spinner plus outcome combinations), including the fixation trials. The averaging procedure produced a separate 20 s fMRI time course for each trial type, averaged across subjects. The reasons for selecting a 20 s duration for the averaging window are as follows.

In previous work (Dale and Buckner, 1997), the delay between stimulus onset and the hemodynamic response has been estimated to be 2 s. If so, then responses specific to the current trial type

occur during the time period beginning 2 s following trial onset and ending 2 s following trial offset; given the trial duration of 12 s, this period ends 14 s following trial onset (see Figure 8).

The normalization procedure corrects for changes in average signal level between runs and removes linear, global trends in average signal levels. However, other changes in average signal levels could cause the baseline to vary across trial types. To allow removal of such changes, an 8 s epoch prior to the beginning of the sampling window was included, bringing the total duration of the sampling window to 20 s. This epoch consists of the six seconds prior to trial onset and the first two seconds of the trial. Given superposition and stationarity, the counterbalancing procedure ensures that the average signal time course during this 8 s epoch is constant across trial types. Subtraction of the median signal level during this 8 s epoch aligns the time courses to a common zero baseline; such methods are used widely in studies of event-related potentials (Regan, 1989).

Talairach Transformation. Each individual's set of infusion images, along with the associated conventional structural scans, were transformed into Talairach space (Breiter et al., 1996a, 1996c; Talairach and Tournoux, 1988) and resliced in the coronal orientation with isotropic voxel dimensions (x, y, z = 3.125 mm). Optimized fit between functional data and structural scans was then obtained via translation of exterior contours.

Averaging across Subjects. To provide the basis for statistical activation maps, Talairach-transformed structural and functional data (i.e., the selectively averaged trials, n = 10) were averaged across the 12 subjects with interpretable BOLD data.

Statistical Mapping, ROI-Based Analysis

Statistical Mapping of Main Effects as ROIs. Data obtained at all time points during the prospect phase of the experiment and all time points collected during the outcome phase of the experiment were statistically evaluated by correlation with a model impulse function (see Figure S3 at http://www.neuron.org/cgi/content/full/30/2/619/DC1) (Boynton et al., 1996; Dale and Buckner, 1997). To eliminate cross-trial hemodynamic overlap, statistical maps were derived from correlation between the γ function and a difference signal, either the time point by time point difference between the prospect data and the fixation epoch data, or the difference between the outcome data and fixation epoch data.

Subsequently, clusters of activation were identified using a cluster-growing algorithm (Bush et al., 1996). In order to maintain an overall $\alpha < 0.05$, this algorithm specifically localized activations that met a corrected p value threshold of $p < 0.007$ for the number of hypothesized brain regions interrogated. Regions of interest (ROIs) were delineated by the voxels with $p < 0.007$ in a 7 mm radius of the voxel with the minimum p value (the "max vox"). Max vox peaks had to fall within a cluster of at least three voxels that met the statistical threshold and to be separated by at least 4 mm from any other putative max vox peak.

Signal Time Course Analysis of ROIs. The normalized fMRI signal was averaged, at each time point, across the voxels within each activation cluster falling within an ROI (Table 1). As described above, the averaged data were assembled into 20 s time courses.

Exploratory Analysis. An exploratory analysis of the time courses was performed in order to examine the across-subject distribution of the averaged fMRI signal in each cluster. Deviation scores from the across subject signal mean were combined across time points and trial types, and displayed as a normal probability ("quantile-quantile") plot for each experimental time period (Chambers, 1983) (see Figure S4 [see supplemental data at http://www.neuron.org/cgi/content/full/30/2/619/DC1]). If the scores of the subjects were distributed normally, as was the case in some but not all clusters, such a plot would be linear. For data deviating from linearity, robust statistical methods were employed to describe the time courses. A test of the relative efficiency of the conventional and robust measures was carried out in order to determine whether robust or conventional least-square statistics were the most appropriate for hypothesis testing; this test is based on the ratio of the mean square error estimates computed using the two methods (see Appendix [http://www.neuron.org/cgi/content/full/30/2/619/DC1]).

Robust Estimation. The robust estimates of location and scale are based on the Tukey bisquare estimator (Hoaglin et al., 1983). This estimator weights scores as a function of their deviation from the sample median. The weights decline smoothly to zero in a bell-shaped fashion as the deviation from the median grows (see Appendix [http://www.neuron.org/cgi/content/full/30/2/619/DC1] for details). As progressively fewer data points receive zero weight, the location estimate approaches the mean (see Appendix).

Baseline Adjustment. The robust estimates of location and scale were computed first from untransformed data. A within-subject subtraction procedure was then used to align the signal time courses for each trial type with a common baseline (see Figure 8 [and Figure S5 on supplemental data at http://www.neuron.org/cgi/content/full/30/2/619/DC1]). In the case of the data to be used for analysis of expectancy responses, the subtrahend consisted of the median fMRI signal during the 6 s prior to trial onset plus the first 2 s of the trial (Figure 8). The median value was then subtracted from the fMRI signals obtained during the subsequent 12 s. In the case of the data to be used for analysis of outcome responses, the subtrahend consisted of the median fMRI signal during the first 6 s of the trial (the prospect phase) plus the first 2 s following presentation of the outcome.

Following the application of the subtraction procedure, new robust estimates of location and scale were computed.

Confidence Intervals. The robust estimates of location and scale were used to compute the (nonsimultaneous) 95% confidence intervals. As recommended by Iglewicz (1983), the number of degrees of freedom was multiplied by 0.7 in constructing confidence intervals about the robust estimates of location.

Hypothesis Testing—Expectancy Phase. The multiple-regression module of RS/Explore was employed to carry out an analysis of variance (ANOVA). In the cases of 12 of the 16 clusters, the data selected for this analysis consisted of the transformed fMRI signals during the period beginning 2 s following trial onset and ending 8 s following trial onset, allowing for a 2 s hemodynamic latency (Dale and Buckner, 1997). Examination of the time courses for these 12 clusters confirmed that signals whose confidence intervals cleared zero did indeed lag the onset of the trial by 2 s. However, in the case of the remaining clusters, the lag was longer (see Figure S2 [see supplemental data at http://www.neuron.org/cgi/content/full/30/2/619/DC1]). For example, the peak signal for GOb(6) occurred at 6 s (Table 2) and was still elevated at 8 s (Figure S2 [see supplemental data]). In the four cases such as this one, the 6 s signal epochs selected for statistical analysis were adjusted to match the time interval during which the peak signal was attained and the area under the curve was maximal (i.e., given a lag of 4 s, time points at 4, 6, and 8 s were used).

Both spinner and time point were defined as categorical (noncontinuous) variables, thus avoiding any assumptions concerning the form of the time courses.

The results of primary interest in the expectancy ANOVA were the main effect of spinner, and the spinner $\times$ time point interaction. A main effect of spinner indicates a difference in the magnitude of the fMRI signals corresponding to the presentation of the three spinners; a spinner $\times$ time point interaction indicates that the form of the signal time courses differed across spinners. Given that ANOVAs were carried out on the signals from 16 different clusters, we used a more stringent α level (0.003) than the conventional 0.05 value as the threshold for a significant effect.

In cases that met the criterion α level, the pair-wise across-spinner contrasts were computed at each of the three time points. Regardless of whether the main effect of spinner or the spinner $\times$ time point interaction met the significance criterion, the confidence band surrounding the location estimate was compared to zero (Tables 1 and 3). Given that multiple comparisons were carried out, simultaneous confidence intervals reflecting the variance at all time points during the expectancy phase were used in this comparison (Tables 1 and 3).

Hypothesis Testing—Outcome Phase. A three-way ANOVA was performed to determine whether the magnitude of the outcome phase responses varied as a function of outcome. In all cases, the data employed fell within a 6 s period beginning 2 s after the onset of the outcome phase. The BOLD signal served as the dependent variable, and spinner, trial type, and time point served as the predictors; trial type, a categorical variable, was nested within spinner. (A $10 win following the presentation of the good spinner constitutes one trial type, whereas a $2.50 win constitutes another.)

Prior to the ANOVA, the expert system was used to determine whether robust or least-square statistics were more efficient and whether the use of variance-adjusted weights was recommended. In all cases, the recommendations of the statistical expert system were accepted.

The results of primary interest in the outcome ANOVA were the main effect of trial type and the trial type * time point interaction. A main effect of trial type indicates a difference in the magnitude of the fMRI signals corresponding to the presentation of the different within-spinner outcomes; a trial type × time point interaction indicates that the form of the signal time course varied across trial type. As in the case of the expectancy phase ANOVAs, the criterion α level was set to 0.003.

In cases that met the criterion α level, pair-wise contrasts were computed between the three trial types within each spinner, at each of the three time points. Regardless of whether the main effect of trial type or the trial type × time point interaction met the significance criterion, the confidence band surrounding the location estimate was compared to zero (Tables 1 and 4). As in the case of the data from the expectancy phase, simultaneous confidence intervals were used in this comparison (Tables 1 and 4).

Statistical Mapping, Post-Hoc Voxel-by-Voxel
Correlational Analysis
This analysis sought to determine if BOLD signals related to the prospects or outcomes could be seen in regions outside the ROIs. Toward this end, statistical maps were generated on averaged data for the correlation between a model impulse (i.e., γ) function and the difference signal produced by subtracting one signal time course from another (i.e., signals from an intermediate condition were subtracted from signals from extreme conditions). Thus, two difference signals were produced for the prospect data, and six difference signals were produced for the outcome data (i.e., by subtracting the response to the middle outcome on each of the three spinners from the responses to the extreme outcomes on that spinner).

Clusters of positive and negative signal change were identified for each correlation between the γ function and a difference signal using the automated cluster growing algorithm described above (Bush et al., 1996). In order to maintain an overall $\alpha < 0.05$, this algorithm specifically localized activation which met a corrected p value threshold for the volume of tissue sampled in a priori regions (i.e., of $p < 4.73 \times 10^{-5}$ for prospects and for outcomes in the NAc, SLEA, amygdala, hypothalamus, VT, and GOb) (Makris et al., 1999). This a priori threshold was computed by summing published volumes for these six brain regions (i.e., 30.97cc) (Makris et al., 1999), dividing this amount by the voxel volume (i.e., 3.125 mm × 3.125 mm × 3 mm = 29.3 mm³) to determine the number of voxels covering these a priori regions (i.e., 1057 voxels), and then dividing $p < 0.05$ by this number of voxels (Breiter et al., 1996a, 1996c). All other regions had to meet a corrected (Bonferroni) threshold for significance of $p < 7.1 \times 10^{-6}$ for the estimated number of voxels sampling brain tissue per subject in this experiment.

Anatomic Localization
Statistical maps of group-averaged data were superimposed over high-resolution conventional T_1-weighted images that had been transformed into the Talairach domain and averaged. Primary anatomic localization of activation foci was based on the Talairach coordinates of the maximum voxel from each activation cluster, with secondary confirmation of this via inspection of the juxtaposition of statistical maps with these coronally resliced T1-weighted structural scans. Confirmation of subcortical localization of activations followed the region of interest conventions described previously (Breiter et al., 1997) for the NAc (previously referred to as the NAc/SCC and here referred to as the NAc due to greater spatial resolution), SLEA (previously referred to as the basal forebrain or BF), amygdala, and VT. The GOb conventions were not described in our previous work and are here delineated. Namely, the GOb (BA 11/47) was identified anteriorly behind the ventral surface of the frontal pole (BA10). It begins with the orbital gyri (anterior, lateral, and medial), which are visible by the beginning of the orbital sulci, and extends posteriorly to the beginning of the SLEA of the basal forebrain, which is visible by the extinguishing of the orbital sulci (transverse orbital sulcus). Laterally, the GOb extends to the anterior horizontal ramus of the Sylvian fissure, and medially, it extends to the olfactory sulcus.

All activations were further checked against the functional image data to ascertain that they did not overlap areas of susceptibility artifact. Such overlap was determined by whether or not the signal intensity in a given voxel during the fixation point condition was less than the average intensity in its slice by 50% of the difference between the average voxel signal intensity in that slice and the average voxel signal intensity outside of that slice.

References

Arvanitogiannis, A., Waraczynski, M., and Shizgal, P. (1996). Effects of excitotoxic lesions of the basal forebrain on MFB self-stimulation. Physiol. Behav. *59*, 795–806.

Arvanitogiannis, A., Tzschentke, T.M., Riscaldino, L., Wise, R.A., and Shizgal, P. (2000). Fos expression following self-stimulation of the medial prefrontal cortex. Behav. Brain Res. *107*, 123–132.

Becerra, L., Breiter, H.C., Jenkins, L., Gonzalez, R.G., and Borsook, D. (2000). Early activation of reward/aversive circuitry following noxious thermal stimuli: temporal response of CNS regions defined by mean field theory analysis. Paper presented at: American Pain Society (Atlanta, GA).

Berns, G.S., Cohen, J.D., and Mintun, M.A. (1997). Brain regions responsive to novelty in the absence of awareness. Science *276*, 1272–1275.

Blackburn, J.R., Pfaus, J.G., and Phillips, A.G. (1992). Dopamine functions in appetitive and defensive behaviours. Prog. Neurobiol. *39*, 247–279.

Bordi, F., and LeDoux, J. (1992). Sensory tuning beyond the sensory system: an initial analysis of auditory response properties of neurons in the lateral amygdaloid nucleus and overlying areas of the striatum. J. Neurosci. *12*, 2493–2503.

Borsook, D., Becerra, L., Aharon, I., Harter, K., Gonzalez, R.G., and Breiter, H.C. (2000). Nucleus accumbens: activation by noxious stimuli in human volunteers. Paper presented at: American Pain Society (Atlanta, GA).

Boynton, G.M., Engel, S.A., Glover, G.H., and Heeger, D.J. (1996). Linear systems analysis of functional magnetic resonance imaging in human V1. J. Neurosci. *16*, 4207–4221.

Breiter, H.C., and Rosen, B.R. (1999). Functional magnetic resonance imaging of brain reward circuitry in the human. NY Acad. Sci. *877*, 523–547.

Breiter, H.C., Etcoff, N.L., Whalen, P.J., Kennedy, W.A., Rauch, S.L., Buckner, R.L., Strauss, M.M., Hyman, S.E., and Rose, B.R. (1996a). Response and habituation of the human amygdala during visual processing of facial expression. Neuron *17*, 875–887.

Breiter, H., Berke, J., Kennedy, W., Rosen, B., and Hyman, S. (1996b). Activation of striatum and amygdala during reward conditioning: an fMRI study. Neuroimage *3*, S220.

Breiter, H.C., Rauch, S.L., Kwong, K.K., Baker, J.R., Weisskoff, R.M., Kennedy, D.N., Kendrick, A.D., Davis, T.L., Jiang, A., Cohen, M.S.,

et al. (1996c). Functional magnetic resonance imaging of symptom provocation in obsessive-compulsive disorder. Arch. Gen. Psychiatry 53, 595–606.

Breiter, H.C., Gollub, R.L., Weisskoff, R.M., Kennedy, D.N., Makris, N., Berke, J.D., Goodman, J.M., Kantor, H.L., Gastfriend, D.R., Riorden, J.P., et al. (1997). Acute effects of cocaine on human brain activity and emotion. Neuron 19, 591–611.

Breiter, H.C., Gollub, R.L., Edmister, W., Talavage, T., Makris, N., Melcher, J., Kennedy, D., Kantor, H., Elman, I., Riorden, J., et al. (1998). Cocaine induced brainstem and subcortical activity observed through fMRI with cardiac gating. Paper presented at: International Society for Magn. Reson. Med. (Sydney, Australia).

Breiter, H.C., Becerra, L., Gonzalez, R.G., Jenkins, L., Huffman, E., Harter, K., Comite, A., and Borsook, D. (2000). Morphine induced reward and pain circuitry activation in drug naïve humans. Paper presented at: American Pain Society (Atlanta, GA).

Brown, V.J., Latimer, M.P., and Winn, P. (1996). Memory for the changing cost of a reward is mediated by the sublenticular extended amygdala. Brain Res. Bull. 39, 163–170.

Bush, G., Jiang, A., Talavage, T., and Kennedy, D. (1996). An automated system for localization and characterization of functional MRI activations in four dimensions. Paper presented at: Second International Conference on Functional Mapping of the Human Brain (Orlando, FL: Academic Press).

Carlezon, W.A., Jr., and Wise, R.A. (1996). Rewarding actions of phencyclidine and related drugs in nucleus accumbens shell and frontal cortex. J. Neurosci. 16, 3112–3122.

Chambers, J.M. (1983). Graphical methods for data analysis (Belmont, CA, and Boston: Wadsworth International Group, Duxbury Press).

Dale, A.M. (1999). Optimal experimental design for event-related fMRI. Hum. Brain Map. 8, 8560–8572.

Dale, A.M., and Buckner, R.L. (1997). Selective averaging of rapidly presented individual trials using fMRI. Hum. Brain Map. 5, 329–340.

Damasio, A.R. (1994). Descartes' Error: Emotion, Reason, and the Human Brain (New York: G.P. Putnam).

Davidson, R.J. (1998). Affective style and affective disorders: Perspectives from affective neuroscience. Cognition and Emotion 12, 307–330.

Davidson, R.J., and Sutton, S.K. (1995). Affective neuroscience: the emergence of a discipline. Curr. Opin. Neurobiol. 5, 217–224.

Davis, M. (1992). The role of the amygdala in conditioned fear. In The Amygdala: Neurobiological Aspects of Emotion, Memory and Mental Dysfunction., J.P. Aggleton, ed. (New York, Wiley-Liss), pp. 255–306.

Elliott, R., Friston, K.J., and Dolan, R.J. (2000). Dissociable neural responses in human reward systems. J. Neurosci. 20, 6159–6165.

Everitt, B.J., and Robbins, T.W. (1992). Amygdala-ventral striatal interactions and reward-related processes. In The Amygdala: Neurobiological Aspects of Emotion, Memory, and Mental Dysfunction, J.P. Aggleton, ed. (New York, Wiley-Liss), pp. 401–429.

Everitt, B.J., Morris, K.A., O'Brien, A., and Robbins, T.W. (1991). The basolateral amygdala-ventral striatal system and conditioned place preference: further evidence of limbic-striatal interactions underlying reward-related processes. Neuroscience 42, 1–18.

Fischl, B., Sereno, M.I., Tootell, R.B., and Dale, A.M. (1999). High-resolution intersubject averaging and a coordinate system for the cortical surface. Hum. Brain Map. 8, 272–284.

Flores, C., Arvanitogiannis, A., and Shizgal, P. (1997). Fos-like immunoreactivity in forebrain regions following self- stimulation of the lateral hypothalamus and the ventral tegmental area. Behav. Brain Res. 87, 239–251.

Francis, S., Rolls, E.T., Bowtell, R., McGlone, F., O'Doherty, J., Browning, A., Clare, S., and Smith, E. (1999). The representation of pleasant touch in the brain and its relationship with taste and olfactory areas. Neuroreport 10, 453–459.

Guarraci, F.A., and Kapp, B.S. (1999). An electrophysiological characterization of ventral tegmental area dopaminergic neurons during differential pavlovian fear conditioning in the awake rabbit. Behav. Brain Res. 99, 169–179.

Hauber, W., Bohn, I., and Giertler, C. (2000). NMDA, but not dopamine D(2), receptors in the rat nucleus accumbens are involved in guidance of instrumental behavior by stimuli predicting reward magnitude. J. Neurosci. 20, 6282–6288.

Heimer, L., Harlan, R.E., Alheid, G.F., Garcia, M.M., and de Olmos, J. (1997). Substantia innominata: a notion which impedes clinical-anatomical correlations in neuropsychiatric disorders. Neuroscience 76, 957–1006.

Hoaglin, D.C., Mosteller, F., and Tukey, J.W. (1983). Understanding Robust and Exploratory Data Analysis (New York: Wiley).

Hollerman, J.R., Tremblay, L., and Schultz, W. (1998). Influence of reward expectation on behavior-related neuronal activity in primate striatum. J. Neurophysiol. 80, 947–963.

Horvitz, J.C. (2000). Mesolimbocortical and nigrostriatal dopamine responses to salient non- reward events. Neuroscience 96, 651–656.

Iglewicz, B. (1983). Robust scale estimators and confidence intervals for location. In Understanding Robust and Exploratory Data Analysis, D.C. Hoaglin, F. Mosteller, and J.W. Tukey, eds. (New York, Wiley), pp. 404–431.

Jiang, A., Kennedy, D., Baker, J., Weisskoff, R.M., Tootell, R., Woods, R., Benson, R.R., Kwong, K., Brady, T.J., Rosen, B.R., and Belliveau, J.W. (1995). Motion detection and correction in functional MR imaging. Hum. Brain Map. 3, 1–12.

Kahneman, D., and Tversky, A. (1979). Prospect theory: an analysis of decision under risk. Econometrica 47, 263–291.

Kapp, B.S., Whalen, P.J., Supple, W.F., and Pascoe, J.P. (1992). Amygdaloid contributions to conditioned arousal and sensory information processing. In The Amygdala: Neurobiological Aspects of Emotion, Memory, and Mental Dysfunction, J.P. Aggleton, ed. (New York: Wiley-Liss), pp. 229–254.

Knutson, B., Westdorp, A., Kaiser, E., and Hommer, D. (2000). FMRI visualization of brain activity during a monetary incentive delay task. Neuroimage 12, 20–27.

LeDoux, J.E. (1992). Emotion and the amygdala. In The Amygdala: Neurobiological Aspects of Emotion, Memory, and Mental Dysfunction, J.P. Aggleton, ed. (New York: Wiley-Liss), pp. 339–351.

LeDoux, J.E. (1994). Emotion, memory and the brain. Scientific American 270, 50–57.

LeDoux, J.E. (1995). Emotion: clues from the brain. Annu. Rev. Psych. 46, 209–235.

LeDoux, J.E. (1996). The Emotional Brain (New York: Simon and Schuster).

Lindvall, O., and Bjorklund, A. (1974). The organization of the ascending catecholamine neuron systems in the rat brain as revealed by the glyoxylic acid fluorescence method. Acta Physiol. Scand. Suppl. 412, 1–48.

Lynd-Balta, E., and Haber, S.N. (1994). The organization of midbrain projections to the ventral striatum in the primate. Neuroscience 59, 609–623.

Makris, N., Meyer, J.W., Bates, J.F., Yeterian, E.H., Kennedy, D.N., and Caviness, V.S. (1999). MRI-Based topographic parcellation of human cerebral white matter and nuclei II. Rationale and applications with systematics of cerebral connectivity. Neuroimage 9, 18–45.

Mellers, B.A., Schwartz, A., Ho, K., and Ritov, I. (1997). Decision affect theory: emotional reactions of the outcomes of risky options. Psychol. Sci. 8, 423–429.

Mellers, B., Schwartz, A., and Ritov, I. (1999). Emotion-based choice. J. Exp. Psychol. Gen. 128, 332–345.

Mirenowicz, J., and Schultz, W. (1996). Preferential activation of midbrain dopamine neurons by appetitive rather than aversive stimuli. Nature 379, 449–451.

Montague, P.R., Dayan, P., and Sejnowski, T.J. (1996). A framework for mesencephalic dopamine systems based on predictive Hebbian learning. J. Neurosci. 16, 1936–1947.

Mora, F., Mogenson, G.J., and Rolls, E.T. (1977). Activity of neurons

in the region of the substantia nigra during feeding in the monkey. Brain Res. *133*, 267–276.

Morris, J.S., Frith, C.D., Perrett, D.I., Rowland, D., Young, A.W., Calder, A.J., and Dolan, R.J. (1996). A differential neural response in the human amygdala to fearful and happy facial expressions. Nature *383*, 812–815.

Nakahara, D., Ishida, Y., Nakamura, M., Kuwahara, I., Todaka, K., and Nishimori, T. (1999). Regional differences in desensitization of c-Fos expression following repeated self-stimulation of the medial forebrain bundle in the rat. Neuroscience *90*, 1013–1020.

O'Doherty, J., Kringelbach, M.L., Rolls, E.T., Hornack, J., and Andrews, C. (2001). Abstract reward and punishment representations in the human orbitofrontal cortex. Nat. Neurosci. *4*, 95–102.

Ono, T., Nishino, H., Sasaki, K., Fukuda, M., and Muramoto, K.I. (1981). Monkey lateral hypothalamic neuron response to sight of food, and during bar press and ingestion. Neurosci. Lett. *21*, 99–104.

Ono, T., Nakamura, K., Nishijo, H., and Fukuda, M. (1986). Hypothalamic neuron involvement in integration of reward, aversion, and cue signals. J. Neurophysiol. *56*, 63–79.

Pfaus, J.G., Damsma, G., Nomikos, G.G., Wenkstern, D.G., Blaha, C.D., Phillips, A.G., and Fibiger, H.C. (1990). Sexual behavior enhances central dopamine transmission in the male rat. Brain Res. *530*, 345–348.

Phillips, M.L., Williams, L., Senior, C., Bullmore, E.T., Brammer, M.J., Andrew, C., Williams, S.C., and David, A.S. (1999). A differential neural response to threatening and non-threatening negative facial expressions in paranoid and non-paranoid schizophrenics. Psych. Res. *92*, 11–31.

Ploghaus, A., Tracey, I., Gati, J.S., Clare, S., Menon, R.S., Matthews, P.M., and Rawlins, J.N. (1999). Dissociating pain from its anticipation in the human brain. Science *284*, 1979–1981.

Quirk, G.J., Repa, C., and LeDoux, J.E. (1995). Fear conditioning enhances short-latency auditory responses of lateral amygdala neurons: parallel recordings in the freely behaving rat. Neuron *15*, 1029–1039.

Redgrave, P., Prescott, T.J., and Gurney, K. (1999a). The basal ganglia: a vertebrate solution to the selection problem? Neuroscience *89*, 1009–1023.

Redgrave, P., Prescott, T.J., and Gurney, K. (1999b). Is the short-latency dopamine response too short to signal reward error? Trends Neurosci. *22*, 146–151.

Reese, T.G., Davis, T.L., and Weisskoff, R.M. (1995). Automated shimming at 1.5T using echo planar image frequency maps. J. Magn. Res. Imag. *5*, 739–745.

Regan, D. (1989). Human brain electrophysiology. Evoked Potentials and Evoked Magnetic Fields in Science and Medicine (New York: Elsevier Press).

Richardson, N., and Gratton, A. (1996). Behavior-relevant changes in nucleus accumbens dopamine transmission elicited by food reinforcement: an electrochemical study in rat. J. Neurosci. *16*, 8160–8169.

Robledo, P., and Koob, G.F. (1993). Two discrete nucleus accumbens projection areas differentially mediate cocaine self-administration in the rat. Behav. Brain Res. *55*, 159–166.

Rogers, R.D., Owen, A.M., Middleton, H.C., Williams, E.J., Pickard, J.D., Sahakian, B.J., and Robbins, T.W. (1999). Choosing between small, likely rewards and large, unlikely rewards activates inferior and orbital prefrontal cortex. J. Neurosci. *19*, 9029–9038.

Rolls, E.T. (1999). The Brain and Emotion (Oxford: University of Oxford Press).

Rolls, E.T. (2000). The orbitofrontal cortex and reward. Cereb. Cortex *10*, 284–294.

Rolls, E.T., Burton, M.J., and Mora, F. (1976). Hypothalamic neuronal responses associated with the sight of food. Brain Res. *111*, 53–66.

Rolls, E.T., Sienkiewicz, Z.J., and Yaxley, S. (1989). Hunger modulates the responses to gustatory stimuli of single neurons in the caudolateral orbitofrontal cortex of the macaque monkey. Eur. J. Neurosci. *1*, 53–60.

Schoenbaum, G., Chiba, A.A., and Gallagher, M. (1998). Orbitofrontal

cortex and basolateral amygdala encode expected outcomes during learning. Nat. Neurosci. *1*, 155–159.

Schoenbaum, G., Chiba, A.A., and Gallagher, M. (1999). Neural encoding in orbitofrontal cortex and basolateral amygdala during olfactory discrimination learning. J. Neurosci. *19*, 1876–1884.

Schoenbaum, G., Chiba, A.A., and Gallagher, M. (2000). Changes in functional connectivity in orbitofrontal cortex and basolateral amygdala during learning and reversal training. J. Neurosci. *20*, 5179–5189.

Schultz, W. (1986). Responses of midbrain dopamine neurons to behavioral trigger stimuli in the monkey. J. Neurophysiol. *56*, 1439–1461.

Schultz, W., and Romo, R. (1990). Dopamine neurons of the monkey midbrain: contingencies of responses to stimuli eliciting immediate behavioral reactions. J. Neurophysiol. *63*, 607–624.

Schultz, W., Apicella, P., Scarnati, E., and Ljungberg, T. (1992). Neuronal activity in monkey ventral striatum related to the expectation of reward. J. Neurosci. *12*, 4595–4610.

Schultz, W., Apicella, P., and Ljungberg, T. (1993). Responses of monkey dopamine neurons to reward and conditioned stimuli during successive steps of learning a delayed response task. J. Neurosci. *13*, 900–913.

Schultz, W., Dayan, P., and Montague, P.R. (1997). A neural substrate of prediction and reward. Science *275*, 1593–1599.

Scott, T.R., Yan, J., and Rolls, E.T. (1995). Brain mechanisms of satiety and taste in macaques. Neurobiology *3*, 281–292.

Shizgal, P. (1997). Neural basis of utility estimation. Curr. Opin. Neurobiol. *7*, 198–208.

Small, D.M., Zatorre, R.J., Dagher, A., Evans, A.C., and Jones-Gotman, M. (2001). Changes in brain activity related to eating chocolate; from pleasure to aversion. Brain, in press.

Stein, E.A., Pankiewicz, J., Harsch, H.H., Cho, J.K., Fuller, S.A., Hoffmann, R.G., Hawkins, M., Rao, S.M., Bandettini, P.A., and Bloom, A.S. (1998). Nicotine-induced limbic cortical activation in the human brain: a functional MRI study. Am. J. Psychiatry *155*, 1009–1015.

Sutton, R.S., and Barto, A.G. (1998). Reinforcement Learning: An Introduction (Cambridge, MA: MIT Press).

Sutton, S.K., and Davidson, R.J. (1997). Prefrontal brain asymmetry: a biological substrate of the behavioral approach and inhibition systems. Psychol. Sci. *8*, 204–210.

Talairach, J., and Tournoux, P. (1988). Co-planar stereotaxic atlas of the human brain (New York: Thieme Medical Publishers).

Thomas, K.M., Devets, W.C., Whalen, P.J., Eccard, C.H., Dahl, R.E., Ryan, N.D., and Casey, B.J. (2001). Amygdala response to facial expressions in children and adults. Biol. Psychiatry *49*, 309–316.

Thut, G., Schultz, W., Roelcke, U., Nienhusmeier, M., Missimer, J., Maguire, R.P., and Leenders, K.L. (1997). Activation of the human brain by monetary reward. Neuroreport *8*, 1225–1228.

Tremblay, L., and Schultz, W. (1999). Relative reward preference in primate orbitofrontal cortex. Nature *398*, 704–708.

Watanabe, M. (1996). Reward expectancy in primate prefrontal neurons. Nature *382*, 629–632.

Wilson, F.A., and Rolls, E.T. (1990). Learning and memory is reflected in the responses of reinforcement-related neurons in the primate basal forebrain. J. Neurosci. *10*, 1254–1267.

Woods, R.P., Cherry, S.R., and Mazziotta, J.C. (1992). Rapid automated algorithm for aligning and reslicing PET images. J. Computer Assisted Tomography *16*, 620–633.

Zald, D.H., Lee, J.T., Fluegel, K.W., and Pardo, J.V. (1998). Aversive gustatory stimulation activates limbic circuits in humans. Brain *121*, 1143–1154.